IN VITRO BIOACTIVITIES OF ANODISED TITANIUM IN MIXTURE OF β-GLYCEROPHOSPHATE AND CALCIUM ACETATE FOR BIOMEDICAL APPLICATION

LEE TE CHUAN

A thesis submitted in
fulfilment of the requirement for the award of the
Doctor of Philosophy of Mechanical Engineering

Faculty of Mechanical and Manufacturing Engineering
Universiti Tun Hussein Onn Malaysia

AUGUST 2016

Special thanks to **my beloved family**,
LEE ING KUANG, LOW CHIEW CHOO, LEE CHING SHEN, LEE CHING JUI, LEE TE HSIANG and also to my family members,
for the love, care, and moral support. Thanks for continuous support for the encouragement toward the success of this study

My inspirational supervisor and co-supervisor,
ASSOC. PROF. DR MAIZLINDA IZWANA BINTI IDRIS &
ASSOC. PROF. DR HASAN ZUHUDI BIN ABDULLAH
for their understanding, support and encouragement during this research

All my friends,
for their concern, encouragement and knowledge.

All the support, enthusiasm and sacrifice in giving me assistance and strength to complete this thesis will never be forgotten.

ACKNOWLEDGMENT

First of all, I would like to thank God for being my strength and courage to do this research

Secondly, I would like to express my sincere appreciation to my supervisor, Assoc. Prof. Dr. Maizlinda Izwana Binti Idris and co-supervisor, Assoc. Prof. Dr. Hasan Zuhudi Bin Abdullah who gave me a good opportunity to do this meaningful research and the support given during this PhD's project. Apart from that, I would like to express my special thanks to Dr Pramod Koshy, lecturer from University of New South Wales, Sydney, Australia, who helps me for proofreading my thesis.

Last but not least, I would like to thank my parents, relatives, and friends for always being supportive of my education especially during this research duration. Thanks again to all who helped me.

ABSTRACT

Anodic oxidation has been widely used to modify the surface properties of titanium in order to improve the biocompatibility after implantation. In this study, high purity titanium foils were exposed in a mixture of β-glycerophosphate disodium salt pentahydrate (β-GP) and calcium acetate monohydrate (CA). The parameters for anodic oxidation method such as applied voltage (50-350 V), current density(10-70 $mA.cm^{-2}$), electrolyte concentration (0.02 M β-GP + 0.2 M CA, 0.04 M β-GP + 0.04 M CA) , anodising time (5-10 mins), agitation speed (300-1500 rpm), ultrasonic amplitude (20-60 μm) and bath temperature (4-100 °C) were varied to investigate the impact on the surface properties of titanium. The results showed that surface of the titanium foil appeared to be highly porous and demonstrated high crystallinity as well as high hydrophilic properties especially when the parameters of anodic oxidation have been varied. This study also proposes two novel methods particularly to accelerate the bone-like apatite formation on the anodised titanium in a shorted time: (1) UV irradiation during *in vitro* testing and (2) adding additives in electrolyte. After soaked and irradiated with UV in simulated body fluid (SBF) for 7 days, highly crystallised bone-like apatite was fully covered on the anodised surface. Interestingly, the smooth and partially porous surface of the anodised titanium was observed to be fully covered by the bone-like apatite layer, which contradict previous research results. The mechanism for growth of bone-like apatite was developed and involved several stages from the existence of hydroxyl groups (•OH) under the UV irradiation has been disclosed thoroughly. Further, additives such as sulphuric acid (H_2SO_4), hydrogen peroxide (H_2O_2) and sodium hydroxide (NaOH) were added into the electrolyte were also able to accelerate the formation of bone-like apatite because of the presence of (•OH), tricalcium phosphate ($Ca_3O_8P_2$), calcium diphosphate ($Ca_2O_7P_2$), calcium titanate ($CaTiO_3$) or sodium titanate ($Na_2Ti_3O_7$) on the anodised surface, which able to induce the nucleation site of bone-like apatite.

ABSTRAK

Pengoksidaan anod telah digunakan secara meluas untuk mengubahsuai sifat-sifat permukaan titanium bagi memperbaiki keserasian bio selepas implitasi. Dalam kajian ini, kerajang titanium berketulenan tinggi telah didedahkan di dalam campuran garam pentahidrat dinatrium β-gliserofosfat (β-GP) dan kalsium asetat monohidrat (CA). Parameter-parameter bagi langkah pengoksidaan anod seperti voltan gunaan (50-350 V), ketumpatan arus (10-70 $mA.cm^{-2}$), kepekatan elektrolit (0.02 M β-GP + 0.2 M CA, 0.04 M β-GP + 0.04 M CA), tempoh penganodan (5-10 mins), kelajuan agitasi (300-1500 rpm), amplitud ultrasonik (20-60 μm) dan suhu elektrolit (4-100 °C) telah diambil kira bagi mengkaji kesan terhadap sifat-sifat permukaan titanium. Permukaan kerajang titanium didapati mempunyai liang yang banyak dan menunjukkan kekristilan serta sifat hidrofilik yang tinggi terutama semasa parameter-parameter pengoksidaan anod telah diubah-ubah. Kajian ini turut mencadangkan dua kaedah baru bagi mempercepatkan pembentukan apatit berbentuk tulang pada titanium yang sudah dianodkan dalam masa yang singkat : (1) penyinaran UV semasa ujian *in vitro* dan (2) peletakan bahan tambahan dalam campuran β-GP + CA. Setelah direndam dan didedahkan dengan UV di dalam SBF selama 7 hari, didapati apatit berbentuk tulang tinggi kekristilan telah dilitupi pada permukaan titanium yang sudah dianodkan. Permukaan titanium tersadur yang licin dan sebahagiannya berliang didapati telah dilitupi sepenuhnya dengan lapisan apatit berbentuk tulang bertentangan dengan dapatan yang. Mekanisma bagi pertumbuhan apatit berbentuk tulang telah dibangunkan dan melibatkan beberapa peringkat bermula dari kewujudan kumpulan hidroksil (•OH) di bawah sinaran UV telah dilampirkan. Bukan itu sahaja, bahan tambahan seperti asid sulfuric (H_2S0_4), hidrogen peroksida (H_2O_2) dan natrium hidroksida (NaOH) ke dalam elektrolit juga berkemampuan untuk mempercepatkan pembentukan apatit berbentuk tulang disebabkan oleh kewujudan kumpulan hidroksil (•OH), trikalsium fosfat ($Ca_3O_8P_2$), di-kalsium difosfat ($Ca_2O_7P_2$), kalsium titanat

($CaTiO_3$) atau natrium titanat ($Na_2Ti_3O_7$) yang berkebolehan untuk mendorong pembentukan tapak penukleusan apatit berbentuk tulang telah dianodkan pada permukaan titanium.

CONTENTS

DECLARATION **i**

DEDICATION **v**

ACKNOWLEDGMENT **vi**

ABSTRACT **vii**

CONTENTS **x**

LIST OF TABLES **xviii**

LIST OF FIGURES **xxii**

LIST OF SYMBOLS AND ABBREVIATIONS **xlv**

CHAPTER 1 INTRODUCTION **1**

1.1 Background 1

1.2 Problem Statements 3

1.3 Objectives 4

1.4 Scope of Study 5

1.5 Significance of Study 6

1.6 Novelty of Study 7

CHAPTER 2 LITERATURE REVIEW **8**

2.1 Introduction 8

2.2 Biomaterials 9

	2.2.1 Overview of Biomaterials	9
	2.2.2 Important Properties of Biomaterials for Implants	12
2.3	Titanium	13
	2.3.1 Metallic Implant Materials	13
	2.3.2 Titanium and its Alloys	14
	2.3.3 Properties of Titanium Implants	15
	2.3.4 Application of Titanium and its Alloy in Biomedical Industry	16
2.4	Titanium Dioxide	19
	2.4.1 Overview of Titanium Dioxide	19
	2.4.2 Polymorphs of Titanium Dioxide	19
	2.4.3 Photocatalytic Properties of Titanium Dioxide	21
	2.4.4 Role of TiO_2 as a Photocatalyst in Biomedical Applications	25
2.5	Calcium Phosphates	28
	2.5.1 Overview of Calcium Phosphate	28
	2.5.2 Osteoinduction of Ca-P Bioceramics	31
	2.5.3 Calcium Acetate	33
	2.5.4 β-Glycerophosphate	35
2.6	Biological Tests	37
	2.6.1 Types of Biological Tests	37
	2.6.2 Simulated Body Fluid (SBF)	38
	2.6.3 Mechanism of Bone-Like Apatite Formation in SBF	40
2.7	Implant Surface	43
	2.7.1 Osseointegration	43

2.7.2 Mechanism of Osseointegration for Titanium Implants 43
2.7.3 Important Features of Implant Surface for Clinical Success 46
2.8 Surface Medication of Titanium and its Alloys 51
2.8.1 Overview of Surface Modification of Titanium and its Alloys 51
2.8.2 Classification of Surface Modification Techniques for Titanium and its Alloys 51
2.8.3 Mechanical Methods 54
2.8.4 Chemical Methods 55
2.8.5 Physical Methods 56
2.8.6 Anodic oxidation 58
2.8.6.1 Overview of Anodic Oxidation 58
2.8.6.2 Mechanism of Anodic Oxidation 60
2.8.6.3 Parameters Affecting the Properties of Oxide Layer 61
2.8.6.4 Anodic oxidation in mixture of β-GP + CA 73

CHAPTER 3 METHODOLOGY 78

3.1 Sample Preparation 78
3.2 Setup of Anodic Oxidation for Different Stirring Methods and Bath Temperatures 78
3.3 UV Light Treatment 82
3.4 *In Vitro* Testing 83
3.4.1 Preparation of SBF 83
3.4.2 Procedures of Bone-Like Apatite Forming Ability Testing 85
3.5 Sample Characterisation 86

3.5.1 Colour Measurement 86

3.5.2 Field Emission Scanning Electron Microscopy (FESEM) 88

3.5.3 Glancing Angle X-ray Diffractometer (GAXRD) 89

3.5.4 Laser Raman Microspectroscopy 90

3.5.5 Atomic Force Microscopy (AFM) 91

3.5.6 Fourier Transform Infrared Spectroscopy (FTIR) 92

3.5.7 Goniometer 93

3.5.8 UV-VIS Spectroscopy 93

3.5.9 Focused Ion Beam (FIB) Milling 95

3.6 Overview of Research Methodology 96

CHAPTER 4 CHARACTERISION AND *IN VITRO* BIOACTIVITY OF ANODISED TITANIUM IN MIXTURE OF β-GP + CA **101**

4.1 Introduction 101

4.2 Colour of Anodised Titanium 102

4.3 Surface Morphology of Anodised Titanium 110

4.4 Surface Morphology of Anodised Titanium 122

4.4.1 GAXRD 122

4.4.2 Laser Raman Microspectroscopy 135

4.5 Surface Topography of Anodised Titanium 139

4.6 Structural Characteristics of Anodised Titanium 147

4.7 Surface Wettability and Surface Energy of Anodised Titanium 148

4.8	Optical Properties of Anodised Titanium	153
4.9	Electrical Behaviour during Anodic Oxidation	156
4.10	*In Vitro* Testing of Anodised Titanium	171

CHAPTER 5 EFFECT OF DIFFERENT STIRRING METHODS AND BATH TEMPERATURES ON SURFACE PROPERTIES OF ANODISED TITANIUM **182**

5.1	Introduction	182
5.2	Observation of Cathode and Anode during Anodic Oxidation	185
5.3	Maximal Voltage during Anodic Oxidation under Different Stirring Methods and Bath Temperatures	190
5.4	Colouration of Anodised Titanium under Different Stirring Methods and Bath Temperatures	194
5.5	Surface Morphology of Anodised Titanium Produced under Different Stirring Methods and Bath Temperatures	196
5.6	Surface Mineralogy of Anodised Titanium under Different Stirring methods and Bath Temperatures	203
5.7	Surface Topography of Anodised Titanium under Different Stirring Methods and Bath Temperatures	211
5.8	Surface Wettability of Anodised Titanium Fabricated under Different Stirring Methods and Bath Temperatures	217

CHAPTER 6 EFFECT OF UV LIGHT TREATMENT ON THE *IN VITRO* BIOACTIVITY OF ANODISED TITANIUM **222**

6.1	Introduction	222

6.2	Colourisation of UV-treated Anodised Titanium	224
6.3	Surface Morphology of UV-Treated Anodised Titanium	225
6.4	Surface Mineralogy of UV-Treated Anodised Titanium	225
6.5	Surface Wettability of UV-Treated Anodised Titanium	231
6.6	*In Vitro* Testing of UV-Treated Anodised Titanium (Without UV Irradiation)	237
6.7	*In Vitro* Testing of UV-Treated Anodised Titanium (With UV Irradiation)	250
6.8	Effect of UV Irradiation on the *In Vitro* Bioactivity of Anodised Titanium	267
6.9	Mechanism of Bone-Like Apatite Formation on Anodised Titanium under UV Irradiation	272

CHAPTER 7 EFFECT OF ADDITIVES IN MIXTURE OF B-GP + CA ELECTROLYTE ON THE *IN VITRO* BIOACTIVITY OF ANODISED TITANIUM **279**

7.1	Introduction	279
7.2	Anodic Oxidation in Mixture of β-GP + CA + H_2SO_4	281
	7.2.1 Colourisation of Anodised Titanium (β- GP + CA + H_2SO_4)	281
	7.2.2 Surface Morphology of Anodised Titanium (β-GP + CA + H_2SO_4)	282
	7.2.3 Surface Mineralogy of Anodised Titanium (β-GP + CA + H_2SO_4)	282
	7.2.4 Surface Topography of Anodised Titanium (β-GP + CA + H_2SO_4)	284
	7.2.5 Structural Characteristics of Anodised Titanium (β-GP + CA + H_2SO_4)	287

	7.2.6 Surface Wettability of Anodised Titanium (β-GP + CA + H_2SO_4)	288
	7.2.7 *In vitro* Testing of Anodised Titanium (β-GP + CA + H_2SO_4)	289
7.3	Anodic Oxidation in Mixture of β-GP + CA + H_2O_2	293
	7.3.1 Colourisation of Anodised Titanium (β-GP + CA + H_2O_2)	293
	7.3.2 Surface Morphology of Anodised Titanium (β-GP + CA + H_2O_2)	294
	7.3.3 Surface Mineralogy of Anodised Titanium (β-GP + CA + H_2O_2)	294
	7.3.4 Surface Topography of Anodised Titanium (β-GP + CA + H_2O_2)	296
	7.3.5 Structural Characteristics of Anodised Titanium (β-GP + CA + H_2O_2)	298
	7.3.6 Surface Wettability of Anodised Titanium (β-GP + CA + H_2O_2)	299
	7.3.7 *In vitro* Testing of Anodised Titanium (β-GP + CA + H_2O_2)	299
7.4	Anodic Oxidation in Mixture of β-GP + CA + $C_2H_4O_2$	303
	7.4.1 Colourisation of Anodised Titanium (β-GP + CA + $C_2H_4O_2$)	303
	7.4.2 Surface Morphology of Anodised Titanium (β-GP + CA + $C_2H_4O_2$)	304
	7.4.3 Surface Mineralogy of Anodised Titanium (β-GP + CA + $C_2H_4O_2$)	304
	7.4.4 Surface Topography of Anodised Titanium (β-GP + CA + $C_2H_4O_2$)	307
	7.4.5 Structural Characteristics of Anodised Titanium (β-GP + CA + $C_2H_4O_2$)	308
	7.4.6 Surface Wettability of Anodised Titanium (β-GP + CA + $C_2H_4O_2$)	309

7.4.7 *In vitro* Testing of Anodised Titanium (β-GP + CA + $C_2H_4O_2$) 311

7.5 Anodic Oxidation in Mixture of β-GP + CA + NaOH 314

7.5.1 Colourisation of Anodised Titanium (β-GP + CA + NaOH) 314

7.5.2 Surface Morphology of Anodised Titanium (β-GP + CA + NaOH) 314

7.5.3 Surface Mineralogy of Anodised Titanium (β-GP + CA + NaOH) 315

7.5.4 Surface Topography of Anodised Titanium (β-GP + CA + NaOH) 318

7.5.5 Structural Characteristics of Anodised Titanium (β-GP + CA + NaOH) 319

7.5.6 Surface Wettability of Anodised Titanium (β-GP + CA + NaOH) 320

7.5.7 *In vitro* Testing of Anodised Titanium (β-GP + CA + NaOH) 321

CHAPTER 8 CONCLUSIONS AND RECOMMENDATIONS 325

8.1 Conclusions 325

8.2 Recommendations 327

REFERENCES 328

APPENDIX 351

Analysis Results 351

List of Publications and Awards 357

LIST OF TABLE

2.1	Advantages and disadvantages of metals, ceramics and polymers for biomedical applications	10
2.2	Example of metal, ceramic, and polymer biomaterial use for biomedical applications	11
2.3	Important properties of biomaterials for use as implants	12
2.4	Comparison of mechanical properties of commonly used metals and its alloys for biomedical applications	13
2.5	Comparison of mechanical properties among titanium and its alloys	14
2.6	Mechanical properties of different grade of Cp Ti	15
2.7	Important properties of titanium in biomedical applications	16
2.8	Properties of rutile, anatase, and brookite TiO_2	21
2.9	Properties of different phases of Ca-P	29
2.10	Properties of calcium acetate	34
2.11	Properties of β-glycerophosphate	36
2.12	Description of each type of *in vitro* and *in vivo* tests	39
2.13	Comparison of the compositions of human blood plasma, original SBF, c-SBF, r-SBF and n-SBF	39
2.14	Definitions of osseointegration	43
2.15	Size range and features of macro rough, micro rough, and nano surface	47
2.16	Previous studies on effect of surface roughness on the clinical success of implants	47
2.17	Previous research on the effect of physicochemical composition on the clinical success of implants	49

2.18	Summary of surface modification methods for titanium and its alloys implants	53
2.19	Example of acid electrolytes and non-acid electrolytes	59
2.20	Experimental parameters of previous studies on anodic oxidation	62
2.21	Summary of conceptual model of oxide layer growth for β-GP + CA electrolyte	76
3.1	Order, amounts, weighting containers, purities and formula weights of reagents for preparing 1000 ml of SBF	83
3.2	Summary of flowcharts of the methodology planned in this thesis	96
4.1	Parameters used for anodic oxidation	102
4.2	Summary for effect of anodic oxidation parameters on surface morphology of anodised titanium	121
4.3	Parameters for study depicted in Figures 4.19-4.24	122
4.4	Parameters used in studies shown in Figure 4.25 to Figure 4.30	128
4.5	Parameters used in studies shown in Figure 4.32 to Figure 4.36	135
4.6	Summary of AFM images of anodised titanium formed in 0.04 M β-GP + 0.4 M CA for 10 minutes at 70 $mA.cm^{-2}$ with varying applied voltages (50-350 V)	143
4.7	Summary of 3D AFM images of anodised titanium formed in 0.04 M β-GP + 0.4 M CA for 10 minutes at 350 V with varying current densities (10-70 $mA.cm^{-2}$)	143
4.8	Conceptual illustration of topography of anodised titanium prepared in mixture of β-GP + CA	146
4.9	Summary of types of electrical behaviour observed during anodisation	156
4.10	Parameters for study depicted in Figures 4.58 to Figure 4.65	158

5.1	Parameters used for investigating the effect of magnetic stirring on the surface properties of anodised titanium	183
5.2	Parameters used for investigating the effect of ultrasonic stirring on surface properties of anodised titanium	183
5.3	Parameters used for investigating the effect of combination stirring on surface properties of anodised titanium	184
5.4	Parameter used for investigating the effect of bath temperature on surface properties of anodised titanium	184
5.5	Descriptions for Figure 5.1 to Figure 5.4	185
5.6	Summary for observations of phenomena at the surface of anode and cathode during anodic oxidation	186
5.7	Summary of GAXRD patterns for Figure 5.18.	205
5.8	Summary of GAXRD patterns for Figure 5.22	209
5.9	Summary of AFM images of the surface of anodised titanium formed at 350 V and 30 $mA.cm^{-2}$ with different agitation speeds	211
5.10	Summary of AFM images of anodised titanium formed at 350 V and 30 $mA.cm^{-2}$ with different ultrasonic amplitude	212
5.11	Summary of AFM images of anodised titanium formed at 350 V and 30 $mA.cm^{-2}$ with different bath temperatures	212
6.1	Parameters used for UV light irradiation	223
6.2	Summary of water contact angles on the anodised surface for series A after UV light treatment	231
6.3	Parameters used in studies shown in Figures 6.17 to 6.20	237
6.4	Summary of UV-treated anodised titanium (AR series) after 7 days immersion in SBF	243
6.5	Summary of surface characteristics of UV-treated anodised samples (series A) after 7 days immersion in SBF	250

6.6	Summary of features observed on the surface of UV-treated anodised samples (series AR) after 7 days immersion in SBF	257
6.7	Parameters used for investigating the effect of UV irradiation on the growth of bone-like apatite	267
6.8	Summary of surface morphologies of UV-treated anodised titanium before and after soaking in SBF under UV irradiation	273
7.1	The composition of electrolyte in volume fraction for anodic oxidation	280
7.2	Summary of GAXRD patterns for Figure 7.3	282
7.3	Summary of GAXRD patterns for Figure 7.5	287
7.4	The summary of surface topography of anodised titanium obtained at 350 V and 70 $mA.cm^{-2}$ for 10 minutes at various volume fraction of 1 M H_2O_2 (12.5-50 vol %)	297
7.5	Summary of GAXRD patterns for Figure 7.19	304
7.6	Summary of GAXRD patterns for Figure 7.27	315

LIST OF FIGURES

1.1	Artificial bone screw	2
1.2	Artificial hip joint	2
2.1	Implants in the human body	10
2.2	Artificial heart value	17
2.3	Artificial vascular stents	17
2.4	Bone screw and bone plate	18
2.5	Commercial dental implant	18
2.6	Structure of rutile TiO_2	20
2.7	Structure of anatase TiO_2	20
2.8	Structure of brookite TiO_2	20
2.9	Band gap for commonly used photocatalysts	23
2.10	Mechanism of the photocatalytic process	24
2.11	Schematic diagram of TiO_2 surface (A) before UV irradiation (B) after UV irradiation	26
2.12	The surface morphology of TiO_2 surface (A) before UV irradiation ,hydrophobic surface (B) after UV irradiation, hydrophilic surface	26
2.13	Surface morphologies of (a) without UV light and (b) with UV light coatings after immersion in SBF for 15 days	27
2.14	Process of mineralisation of collagen fibril, (A) stable mineral droplet. (B) binding to distinct region, (C) diffusion into fibril, (E) solidification and mineralisation of fibril	32
2.15	Molecular events in osteogenic process	32
2.16	Chemical structure of calcium acetate	33

2.17	Different types of fish skin gelatin scaffolds. G: simple gelatin; GC: gelatin + chitosan; GCA: gelatin + calcium acetate; GCCA: gelatin + chitosan + calcium acetate	34
2.18	SEM images of the microstructure of different types of gelatin scaffolds G: simple gelatin; GC: gelatin + chitosan; GCA: gelatin + calcium acetate; GCCA: gelatin + chitosan + calcium acetate	34
2.19	Chemical structure of β-glycerophosphate	35
2.20	SEM images of the hydrogels prepared by using different ratios of chitosan/α,β glycerophosphate (S1) 0.18% chitosan solution 9.6 mL; 50% α,β glycerophosphate solution 0.4 ml (S2) 0.18% chitosan solution 9.6 mL; 50% α,β glycerophosphate solution 1.0 ml (S3) 0.18% chitosan solution 8.4 mL; 50% α,β glycerophosphate solution 1.6 mL	36
2.21	Classification of biological tests	38
2.22	Ion exchange between the Ti-OH group and Ca^{2+}	40
2.23	Formation of amorphous calcium phosphate	40
2.24	Ion exchange between the amorphous calcium phosphate and Na^{+} and Mg^{2+} ions	41
2.25	Formation of bone-like apatite on the surface of TiO_2 in SBF	41
2.26	SEM images of the surface of polyetheretherketone surface after soaking in 1.5 SBF for 4 weeks	42
2.27	Surface morphology of laser-cladded coating on Ti–6Al–4V soaked in SBF for 14 days	42
2.28	The illustration of osseointegration between implant and tissue	45
2.29	SEM micrographs showing MC3T3-E1 osteoblastic cell morphology after 2 days of culture on (A) Smooth-Ti, (B) Alumina–Ti, (C) SLA and (D) BCP–Ti	48

2.30	SEM micrographs of various as-deposited TiO_2 thin films immersed in SBF for 12 weeks at 37 °C, (A) Amorphous, (B) Mixed (Rutile/Anatase), (C) Rutile and (D) Anatase	50
2.31	Classification of the surface modification technologies for titanium and its alloys	52
2.32	Dependence of yield stress and ultimate tensile strength on the peak current applied during EDM process	54
2.33	Surface morphologies of Ti and Nb alkali-heat-treated at different temperatures	56
2.34	Surface morphology of PVD coated surfaces on Ti-6Al-4V: SEM (a)–(c) and AFM (d)–(f) images of CrN (a) and (d), CrN/NbN superlattice (b) and (e) and WC/C (c) and (f)	57
2.35	Schematic diagram of anodic oxidation (1) D.C. power supply, (2) Ti anode (3) Ti cathode (4) cooling water (5) magnetic stirrer bar (6) thermometer, and (7) jacketed beaker	59
2.36	SEM surface morphologies of Ti surfaces treated with MAO at different voltages: (A) 190 V, (B) 230 V, (C) 270 V, (D) 350 V, (E) 450V and (F) 600 V	67
2.37	XRD diffractograms for untreated Ti and the samples anodically oxidized using current densities of 150 and 300 mA/cm^2. Ti = titanium, A = anatase R = rutile and HA = hydroxyapatite	68
2.38	TF-XRD patterns of titanium metals anodically oxidised at 155V in H_2SO_4 with concentration of (A) 0.5M, (B) 1 M, (C) 3 M for 1 min	68
2.39	Surface morphologies of PEO coatings: (a) 1 min, (b) 5 min, (c) 10 min, (d) 20 min, (e) 40 min, (f) 60 min and (g) 120 min	69
2.40	Surface morphology of anodised titanium prepared in different electrolyte (A) H_2SO_4 (B) $C_2H_4O_2$ (C) H_3PO_4 (D) Na_2SO_4 (E) NH_4F + ethylene glycol	70

2.41	Average surface roughness of samples produced by different ultrasonic power intensities	71
2.42	EDS compositional analysis of (a) MAO (b) MAO-180 (c) MAO-250 and (d) MAO-350 samples	71
2.43	SEM images of the films prepared at 30 V in 2 M NaOH solutions at different temperatures (A) 20 °C (B) 40 °C (C) 60 °C	72
2.44	Cross-sectional SEM images of the films prepared at 30 V in 2 M NaOH solutions at different temperatures (A) 20 °C (B) 40 °C (C) 60 °C	72
2.45	SEM micrograph of anodised titanium formed in β-GP + CA electrolyte	74
2.46	XRD patterns of the anodised titanium obtained at (A) 250, (B) 350 and (C) 450 V	74
2.47	FIB micrographs showing the cross sectional regions for anodised samples at 10 $mA.cm^{-2}$ and 20 $mA.cm^{-2}$ for 10 minutes in mixture of β-GP + CA	75
2.48	Conceptual model of oxide layer growth for β-GP + CA electrolyte	76
2.49	FESEM images of the samples anodised in 0.02 M β-GP + 0.2 M CA, current densities 10 and 20 $mA.cm^{-2}$ at 150 and 350 V for 10 min after soaking in SBF for 7 days	77
3.1	Schematic diagram of anodic oxidation under magnetic stirring	79
3.2	Schematic diagram of anodic oxidation under ultrasonic stirring	80
3.3	Schematic diagram of anodic oxidation under combination stirring	80
3.4	Schematic diagram of anodic oxidation at bath temperature of 4°C	81
3.5	Schematic diagram of anodic oxidation at bath temperatures of 40°-100°C	81
3.6	Schematic diagram showing UV light treatment	82

3.7	Schematic diagram of *in vitro* testing with UV light irradiation	86
3.8	Interface of EasyRGB colour conversion software	87
3.9	Schematic diagram of FESEM	88
3.10	Schematic diagram of X-ray penetration of GAXRD	89
3.11	Schematic diagram of a laser Raman spectrometer device	90
3.12	Schematic of AFM instrument showing "beam bounce" method of detection using a laser and position sensitive photodiode detector	91
3.13	Schematic diagram of the FTIR spectrometer	92
3.14	Schematically of Young-Laplace equation using surface tension vectors for a liquid on a solid substrate	93
3.15	Schematic graphs of (a) working principle of UV-Vis spectroscopy, (b) simple geometry of UV-Vis spectroscopy system	94
3.16	Schematic diagram showing the configuration of a dual beam focused ion beam system	95
3.17	Flowchart of methodology for achieving 1st and 2nd objectives	97
3.18	Flowchart of methodology for achieving 3rd objective	98
3.19	Flowchart of methodology for achieving 4th and 5th objectives	99
3.20	Flowchart of methodology for achieving 6th objective	100
4.1	Multi beam interference responsible for colour of anodised titanium	103
4.2	Colours of anodised titanium (0.02 M β-GP + 0.2 M CA, 5 minutes) as a function of the current density and the applied voltage	104
4.3	Colours of anodised titanium (0.02 M β-GP + 0.2 M CA, 5 minutes) as a function of the current density and the applied voltage (conversion of CIELAB using computer software)	104

4.4	Colours of anodised titanium (0.02 M β-GP + 0.2 M CA, 10 minutes) as a function of the current density and the applied voltage	105
4.5	Colours of anodised titanium (0.02 M β-GP + 0.2 M CA, 10 minutes) as a function of the current density and the applied voltage (conversion of CIELAB using computer software)	106
4.6	Colours of anodised titanium (0.04 M β-GP + 0.4 M CA, 5 minutes) as a function of the current density and the applied voltage	107
4.7	Colours of anodised titanium by conversion of CIELAB for Figure 4.6	108
4.8	Colours of anodised titanium (0.04 M β-GP + 0.4 M CA, 10 minutes) as a function of the current density and the applied voltage	108
4.9	Colours of anodised titanium by conversion of CIELAB for Figure 4.8	108
4.10	Colour sequence of anodised titanium in mixture of β-GP + CA	109
4.11	FESEM micrographs of anodised titanium formed at varying voltages (50-350 V) in 0.02 M β-GP + 0.2 M CA for 10 minutes at 10 and 70 $mA.cm^{-2}$	113
4.12	FESEM micrographs of anodised titanium formed at varying voltages (50-350 V) in 0.04 M β-GP + 0.4 M CA for 10 minutes at 10 and 70 $mA.cm^{-2}$	114
4.13	FESEM micrographs of anodised titanium formed at varying current densities (10-70 $mA.cm^{-2}$).in 0.02 M β-GP + 0.2 M CA for 10 minutes at 50 and 350 V	115
4.14	FESEM micrographs of anodised titanium formed at varying current densities (10-70 $mA.cm^{-2}$).in 0.04 M β-GP + 0.4 M CA for 10 minutes at 50 and 350 V	116

4.15	FESEM micrographs of anodised titanium formed in 0.02 M β-GP + 0.2 M CA for 350 V at 10-70 $mA.cm^{-2}$ for varying anodising times (5 and 10 minutes)	117
4.16	FESEM micrographs of anodised titanium formed in 0.04 M β-GP + 0.4 M CA for 350 V at 10-70 $mA.cm^{-2}$ for varying anodising times (5 and 10 minutes)	118
4.17	FESEM micrographs of anodised titanium formed at 70 $mA.cm^{-2}$, 50-350 V with varying electrolyte concentrations (0.02 M β-GP + 0.2 M CA and 0.04 M β-GP + 0.4 M CA)	119
4.18	Schematic diagram showing the porous titanium oxide formation above the breakdown potential: (A) oxide growth to maximal thickness, (B) breakage of oxide layer by the formation of crystallites (pore formation), (C) immediate repassivation of pore tips, (D) breakdown of the repassivated oxide, and (E) dissolution of the formed oxide and second repassivation	121
4.19	GAXRD patterns of the samples anodised in 0.02 M β-GP + 0.2 M CA, current density 10 $mA.cm^{-2}$ at 50-350 V for 10 minutes	124
4.20	GAXRD patterns of the samples anodised in 0.02 M β-GP + 0.2 M CA, current density 70 $mA.cm^{-2}$ at 50-350 V for 10 minutes	124
4.21	GAXRD patterns of the samples anodised in 0.02 M β-GP + 0.2 M CA, current density 70 $mA.cm^{-2}$ at 50-350 V for 5 minutes	125
4.22	GAXRD patterns of the samples anodised in 0.02 M β-GP + 0.2 M CA, applied voltage of 50 V at 10-70 $mA.cm^{-2}$ for 10 minutes	127
4.23	GAXRD patterns of the samples anodised in 0.02 M β-GP + 0.2 M CA, applied voltage of 350 V at 10-70 $mA.cm^{-2}$ for 10 minutes	127

4.24	GAXRD patterns of the samples anodised in 0.02 M β-GP + 0.2 M CA, applied voltage of 350 V at 10-70 $mA.cm^{-2}$ for 5 minutes	128
4.25	GAXRD patterns of the samples anodised in 0.04 M β-GP + 0.4 M CA, current density 10 $mA.cm^{-2}$ at 50-350 V for 10 minutes	130
4.26	GAXRD patterns of the samples anodised in 0.04 M β-GP + 0.4 M CA, current density 70 $mA.cm^{-2}$ at 50-350 V for 10 minutes	130
4.27	GAXRD patterns of the samples anodised in 0.04 M β-GP + 0.4 M CA, current density 70 $mA.cm^{-2}$ at 50-350 V for 5 minutes	131
4.28	GAXRD patterns of the samples anodised in 0.04 M β-GP + 0.4 M CA, applied voltage of 50 V at 10-70 $mA.cm^{-2}$ for 10 minutes	132
4.29	GAXRD patterns of the samples anodised in 0.04 M β-GP + 0.4 M CA, applied voltage of 350 V at 10-70 $mA.cm^{-2}$ for 10 minutes	132
4.30	GAXRD patterns of the samples anodised in 0.04 M β-GP + 0.4 M CA, applied voltage of 350 V at 10-70 $mA.cm^{-2}$ for 5 minutes	133
4.31	GAXRD patterns of the samples anodised in various electrolyte concentration (0.02 M β-GP + 0.2 M CA and 0.04 M β-GP + 0.4 M CA) and applied voltage (250 V and 350 V) at 70 $mA.cm^{-2}$ for 10 minutes	134
4.32	Raman spectra of the samples anodised in 0.02 M β-GP + 0.2 M CA, current density 70 $mA.cm^{-2}$ at 50-350 V for 10 minutes	136
4.33	Raman spectra of the samples anodised in 0.04 M β-GP + 0.4 M CA, current density 70 $mA.cm^{-2}$ at 50-350 V for 10 minutes	137

4.34	Raman spectra of the samples anodised in 0.02 M β-GP + 0.2 M CA, applied voltage of 350 V at 10-70 mA.cm^{-2} for 10 minutes	137
4.35	Raman spectra of the samples anodised in 0.04 M β-GP + 0.4 M CA, applied voltage of 350 V at 10-70 mA.cm^{-2} for 10 minutes	138
4.36	Raman spectra patterns of the samples anodised in various electrolyte concentration (0.02 M β-GP + 0.2 M CA and 0.04 M β-GP + 0.4 M CA) and applied voltage (250 V and 350 V) at 70 mA.cm^{-2} for 10 minutes	139
4.37	Average surface roughness of anodised titanium prepared in 0.02 M β-GP + 0.2 M CA for 10 minutes	140
4.38	Average surface roughness of anodised titanium prepared in 0.04 M β-GP + 0.4 M CA for 10 minutes	141
4.39	3D AFM images of anodised titanium formed at varying applied voltage (50-350 V) in 0.04 M β-GP + 0.4 M CA for 10 minutes at 70 mA.cm^{-2}	142
4.40	3D AFM images of anodised titanium formed at varying applied voltage (10-70 mA.cm^{-2}) in 0.04 M β-GP + 0.4 M CA for 10 minutes at 350 V	142
4.41	Average surface roughness of anodised titanium formed in 0.04 M β-GP + 0.4 M CA for 50-350 V at 70 mA.cm^{-2} with varying anodising times (5 and 10 minutes)	144
4.42	Average surface roughness of anodised titanium formed at 70 mA.cm^{-2}, 50-350 V with varying electrolyte concentrations (0.02 M β-GP + 0.2 M CA and 0.04 M β-GP + 0.4 M CA)	144
4.43	3D AFM images of anodised titanium formed in 0.04 M β-GP + 0.4 M CA for 250 V and 350 V at 70 mA.cm^{-2} with varying anodising times (5 and 10 minutes)	145
4.44	3D AFM images of anodised titanium formed at 50 mA.cm^{-2} and 70 mA.cm^{-2} at 350 V with varying	145

	electrolyte concentrations (0.02 M β-GP + 0.2 M CA and 0.04 M β-GP + 0.4 M CA)	
4.45	FTIR spectra of anodised titanium formed at 70 mA.cm^{-2}, 50-350 V in 0.04 M β-GP + 0.4 M CA for 10 minutes	147
4.46	Images of water on the anodised titanium after anodisation at voltages of (A) 50 V, (B) 150 V, (C) 250 V, and (D) 350 V at 70 mA.cm^{-2} in 0.02 M β-GP + 0.2 M CA for 10 minutes	148
4.47	Images of water on the anodised titanium after anodisation at current density of (A) 10 mA.cm^{-2}, (B) 30 mA.cm^{-2}, (C) 50 mA.cm^{-2}, and (D) 70 mA.cm^{-2} at 350 V in 0.02 M β-GP + 0.2 M CA for 10 minutes	149
4.48	Images of water on the anodised titanium after anodisation at voltages of (A) 50 V, (B) 150 V, (C) 250 V, and (D) 350 V at 70 mA.cm^{-2} in 0.04 M β-GP + 0.4 M CA for 10 minutes	150
4.49	Images of water on the anodised titanium after anodisation at current densities of (A) 10 mA.cm^{-2}, (B) 30 mA.cm^{-2}, (C) 50 mA.cm^{-2}, and (D) 70 mA.cm^{-2} at 350 V in 0.04 M β-GP + 0.4 M CA for 10 minutes	151
4.50	Graph of surface energy versus current density for the coating produced by anodising titanium at a applied voltage of 350 V for 10 minutes in mixture of 0.04 M β-GP + 0.4 M CA	152
4.51	Graph of surface energy versus applied voltage for the coating produced by anodising titanium at a current density of 70 mA.cm^{-2} for 10 minutes in mixture of 0.04 M β-GP + 0.4 M CA	153
4.52	Plot of $(Ahv)^2$ versus hv for the anodised titanium at 350V and 70mA.cm^{-2} for 10 minutes	154
4.53	Band gap of the samples anodised in 0.04 M β-GP + 0.4 M CA, current density 70 mA.cm^{-2} at 50-350 V for 10 minutes	154

4.54	Band gap of the samples anodised in 0.04 M β-GP + 0.4 M CA, applied voltage of 350 V at 10-70 $mA.cm^{-2}$ for 10 minutes	155
4.55	Voltage-current density versus time graph for Type A electrical behaviour	157
4.56	Voltage-current density versus time graph for Type B electrical behaviour	157
4.57	Voltage-current density versus time graph for Type C electrical behaviour	158
4.58	Voltage-current density versus time graph of the samples anodised in 0.02 M β-GP + 0.2 M CA and current density of 10 $mA.cm^{-2}$ at 50-350 V for 10 minutes	159
4.59	Voltage-current density versus time graph of the samples anodised in 0.02 M β-GP + 0.2 M CA and current density of 70 $mA.cm^{-2}$ at 50-350 V for 10 minutes	160
4.60	Voltage-current density versus time graph of the samples anodised in 0.02 M β-GP + 0.2 M CA and applied voltage of 50 V at 10-70 $mA.cm^{-2}$ for 10 minutes.	161
4.61	Voltage-current density versus time graph of the samples anodised in 0.02 M β-GP + 0.2 M CA and applied voltage of 350 V at 10-70 $mA.cm^{-2}$ for 10 minutes	162
4.62	Voltage-current density versus time graph of the samples anodised in 0.04 M β-GP + 0.04 M CA and current density of 10 $mA.cm^{-2}$ at 50-350 V for 10 minutes	163
4.63	Voltage-current density versus time graph of the samples anodised in 0.04 M β-GP + 0.4 M CA and current density of 70 $mA.cm^{-2}$ at 50-350 V for 10 minutes	164
4.64	Voltage-current density versus time graph of the samples anodised in 0.04 M β-GP + 0.4 M CA and applied voltage of 50 V at 10-70 $mA.cm^{-2}$ for 10 minutes	165
4.65	Voltage-current density versus time graph of the samples anodised in 0.04 M β-GP + 0.4 M CA and applied voltage of 350 V at 10-70 $mA.cm^{-2}$ for 10 minutes	166

4.66	Electrical behaviour of samples prepared in 0.02 M β-GP + 0.2 M CA as a function of the applied voltage and current density	167
4.67	Electrical behaviour of samples prepared in 0.04 M β-GP + 0.4 M CA as a function of the applied voltage and current density	167
4.68	The conceptual model of oxide growth for electrical behaviour Type A	168
4.69	Conceptual model of oxide growth for electrical behaviour Type B	169
4.70	Conceptual model of oxide growth for electrical behaviour Type C	170
4.71	FESEM images of anodised titanium formed at different applied voltages (A) 50 V (B) 150 V (C) 250 V, and (D) 350 V after soaking in SBF for 7 days without UV irradiation	173
4.72	FESEM images of anodised titanium formed at different applied voltages (A) 50 V (B) 150 V (C) 250 V, and (D) 350 V after soaking in SBF for 7 days with UVC irradiation	174
4.73	FESEM images of anodised titanium formed at different applied voltages (A) 50 V (B) 150 V (C) 250 V, and (D) 350 V after soaking in SBF for 7 days with UVA irradiation	175
4.74	GAXRD patterns of anodised titanium at 50-350 V after soaking in SBF for 7 days with UVC irradiation	176
4.75	GAXRD patterns of anodised titanium at 50-350 V after soaking in SBF for 7 days with UVA irradiation	177
4.76	FTIR spectra of anodised titanium at 50-350 V after soaking in SBF for 7 days with UVC irradiation	178
4.77	FTIR spectra of anodised titanium at 50-350 V after soaking in SBF for 7 days with UVA irradiation	178

4.78	Schematic showing the mechanism of bone-like apatite formation on the anodised metal surface immersed in SBF under UV light irradiation	181
5.1	Schematic diagrams showing the phenomena at the cathode and anode at different agitation speeds	187
5.2	Schematic diagrams showing the phenomena at the cathode and anode at different ultrasonic amplitudes	188
5.3	Schematic diagrams showing the phenomena at the cathode and anode for combination stirring	189
5.4	Schematic diagrams showing the phenomena at the cathode and anode at different bath temperatures	190
5.5	Recorded maximal voltage during anodic oxidation at 30 $mA.cm^{-2}$ in 0.04 M β-GP + 0.4 M CA for 10 minutes at different agitation speeds	191
5.6	Recorded maximal voltage during anodic oxidation at 30 $mA.cm^{-2}$ in 0.04 M β-GP + 0.4 M CA for 10 minutes at different ultrasonic amplitudes	192
5.7	Recorded maximal voltage during combination stirring of anodic oxidation at 30 $mA.cm^{-2}$ in 0.04 M β-GP + 0.4 M CA for 10 min	193
5.8	Recorded maximal voltage during anodic oxidation at 30 $mA.cm^{-2}$ in 0.04 M β-GP + 0.4 M CA for 10 minutes at different bath temperatures	193
5.9	Colour of anodised titanium produced at 350 V and 30 $mA.cm^{-2}$ for 10 minutes at different agitation speeds	195
5.10	Colour of anodised titanium produced at 350 V and 30 $mA.cm^{-2}$ for 10 minutes at different ultrasonic amplitudes	195
5.11	Colour of anodised titanium produced at 350 V and 30 $mA.cm^{-2}$ for 10 minutes with different combination stirring settings	196
5.12	Colour of anodised titanium produced at 350 V and 30 $mA.cm^{-2}$ for 10 minutes at different temperatures	196

5.13	FESEM micrographs of anodised titanium at 350V, 30 $mA.cm^{-2}$ for 10 minutes in mixture of 0.04 M β-GP + 0.4 M CA at different agitation speeds	199
5.14	FESEM micrographs of anodised titanium at 350V, 30 $mA.cm^{-2}$ for 10 minutes in mixture of 0.04 M β-GP + 0.4 M CA at different ultrasonic amplitudes	200
5.15	FESEM micrographs of anodised titanium at 350V, 30 $mA.cm^{-2}$ for 10 minutes in mixture of 0.04 M β-GP + 0.4 M CA (combination of magnetic stirring and ultrasonic stirring)	201
5.16	FESEM micrographs of anodised titanium at 350V, 30 $mA.cm^{-2}$ for 10 minutes in mixture of 0.04 M β-GP + 0.4 M CA at different bath temperature	202
5.17	GAXRD patterns of anodised titanium fabricated at 350 V and 30 $mA.cm^{-2}$ for 10 minutes using different agitation speeds	204
5.18	GAXRD patterns of anodised titanium fabricated at 350 V and 30 $mA.cm^{-2}$ for 10 minutes under different ultrasonic amplitudes	205
5.19	GAXRD patterns of anodised titanium fabricated at 350 V, 30 $mA.cm^{-2}$ at an ultrasonic amplitude of 20 μm for 10 minutes at different agitation speeds	207
5.20	GAXRD patterns of anodised titanium fabricated at 350 V, 30 $mA.cm^{-2}$ at an ultrasonic amplitude of 30 μm for 10 minutes at different agitation speeds	207
5.21	GAXRD patterns of anodised titanium fabricated at 350 V, 30 $mA.cm^{-2}$ at an ultrasonic amplitude of 40 μm for 10 minutes at different agitation speeds	208
5.22	GAXRD patterns of anodised titanium fabricated at 350 V, 30 $mA.cm^{-2}$ for 10 minutes at different bath temperatures	210

5.23	Surface topography of anodised titanium fabricated at 350V, 30 mA.cm^{-2} for 10 minutes in mixture of 0.04 M β-GP + 0.4 M CA at different agitation speeds	214
5.24	Surface topography of anodised titanium fabricated at 350V, 30 mA.cm^{-2} for 10 minutes in mixture of 0.04 M β-GP + 0.4 M CA at different ultrasonic amplitudes	215
5.25	Surface topography of anodised titanium fabricated at 350V, 30 mA.cm^{-2} for 10 minutes in mixture of 0.04 M β-GP + 0.4 M CA at different bath temperatures	216
5.26	Images of water on anodised titanium fabricated at 350V, 30 mA.cm^{-2} for 10 minutes in mixture of 0.04 M β-GP + 0.4 M CA at different agitation speeds	218
5.27	Images of water on anodised titanium fabricated at 350V, 30 mA.cm^{-2} for 10 minutes in mixture of 0.04 M β-GP + 0.4 M CA at different ultrasonic amplitudes	220
5.28	Images of water on anodised titanium fabricated at 350V, 30 mA.cm^{-2} for 10 minutes in mixture of 0.04 M β-GP + 0.4 M CA at different bath temperatures	221
6.1	Colours of anodised titanium for A series as a function of UV light treatment duration and pH of solution after UV light treatment	224
6.2	Colours of anodised titanium for AR series as a function of the UV light treatment duration and pH of solution after UV light treatment	224
6.3	Surface morphology of anodised titanium for series A as a function of the UV light treatment duration and pH of solution during the UV light treatment	226
6.4	Surface morphology of anodised titanium for series AR as a function of the UV light treatment duration and pH of solution during the UV light treatment	227
6.5	GAXRD patterns of anodised titanium for series A after UV light treatment for 4 h at different pH values	228

6.6	GAXRD patterns of anodised titanium for series A after UV light treatment for 8 h at different pH values	228
6.7	GAXRD patterns of anodised titanium for series A after UV light treatment for 12 h at different pH values	229
6.8	GAXRD patterns of anodised titanium for series AR after UV light treatment for 4 h at different pH values	229
6.9	GAXRD patterns of anodised titanium for series AR after UV light treatment for 8 h at different pH values	230
6.10	GAXRD patterns of anodised titanium for series AR after UV light treatment for 12 h at different pH values	230
6.11	Images of water on anodised titanium for series A after UV light treatment for 4 h at different pH of solution (A) pH 1 (B) pH 4 (C) pH 7 and (D) pH 11	232
6.12	Images of water on anodised titanium for series A after UV light treatment for 8 hours at different pH of solution (A) pH 1 (B) pH 4 (C) pH 7 and (D) pH 11	232
6.13	Images of water on anodised titanium for series A after UV light treatment for 12 hours at different pH of solution (A) pH 1 (B) pH 4 (C) pH 7 and (D) pH 11	233
6.14	Images of water on anodised titanium for series AR after UV light treatment for 4 hours at different pH of solution (A) pH 1 (B) pH 4 (C) pH 7 and (D) pH 11	235
6.15	Images of water on anodised titanium for series AR after UV light treatment for 8 hours at different pH of solution (A) pH 1 (B) pH 4 (C) pH 7 and (D) pH 11	235
6.16	Images of water on anodised titanium for series AR after UV light treatment for 12 hours at different pH of solution (A) pH 1 (B) pH 4 (C) pH 7 and (D) pH 11	236
6.17	FESEM images of 4 h UV-treated anodised titanium (series A) in solution of (A) pH 1 (B) pH 4 (C) pH 7 and (D) pH 11 after soaking in SBF for 7 days without UV irradiation	238

6.18	FESEM images of 8 h UV-treated anodised titanium (series A) in solution of (A) pH 1 (B) pH 4 (C) pH 7 and (D) pH 11 after soaking in SBF for 7 days without UV irradiation	239
6.19	FESEM images of 12 h UV-treated anodised titanium (series A) in solution of (A) pH 1 (B) pH 4 (C) pH 7 and (D) pH 11 after soaking in SBF for 7 days without UV irradiation	240
6.20	FESEM images of UV-treated anodised titanium (series A) in solution of pH 1 with (A) 4 hours (B) 8 hours and (C) 12 hours after soaking in SBF for 7 days without UV irradiation	241
6.21	FESEM images of 4h UV-treated anodised titanium (series AR) in solution of (A) pH 1 (B) pH 4 (C) pH 7 and (D) pH 11 after soaking in SBF for 7 days without UV irradiation	244
6.22	FESEM images of 8 h UV-treated anodised titanium (series AR) in solution of (A) pH 1 (B) pH 4 (C) pH 7 and (D) pH 11 after soaking in SBF for 7 days without UV irradiation	245
6.23	FESEM images of 12 h UV-treated anodised titanium (series AR) in solution of (A) pH 1 (B) pH 4 (C) pH 7 and (D) pH 11 after soaking in SBF for 7 days without UV irradiation	246
6.24	FESEM images of UV-treated anodised titanium (series AR) in solution of pH 1 with (A) 4 hours (B) 8 hours and (C) 12 hours after soaking in SBF for 7 days without UV irradiation	247
6.25	GAXRD patterns of 12 h UV-treated anodised titanium (A series) in solution of (A) pH 1 (B) pH 4 (C) pH 7 and (D) pH 11 after soaking in SBF for 7 days without UV irradiation	248

6.26	GAXRD patterns of 12 h UV-treated anodised titanium (AR series) in solution of (A) pH 1 (B) pH 4 (C) pH 7 and (D) pH 11 after soaking in SBF for 7 days without UV irradiation.	249
6.27	FESEM images of 4 h UV-treated anodised titanium (series A) in solutions of (A) pH 1 (B) pH 4 (C) pH 7 and (D) pH 11 after soaking in SBF for 7 days with UV irradiation	252
6.28	FESEM images of 8 h UV-treated anodised titanium (series A) in solutions of (A) pH 1 (B) pH 4 (C) pH 7 and (D) pH 11 after soaking in SBF for 7 days with UV irradiation	253
6.29	FESEM images of 12 h UV-treated anodised titanium (series A) in solutions of (A) pH 1 (B) pH 4 (C) pH 7 and (D) pH 11 after soaking in SBF for 7 days with UV irradiation	254
6.30	FESEM images of UV-treated anodised titanium (series A) in solution of pH 1 with (A) 4 hours (B) 8 hours and (C) 12 hours after soaking in SBF for 7 days with UV irradiation	255
6.31	FESEM images of 4 h UV-treated anodised titanium (series AR) in solutions of (A) pH 1 (B) pH 4 (C) pH 7 and (D) pH 11 after soaking in SBF for 7 days with UV irradiation	258
6.32	FESEM images of 8 h UV-treated anodised titanium (series AR) in solutions of (A) pH 1 (B) pH 4 (C) pH 7 and (D) pH 11 after soaking in SBF for 7 days with UV irradiation	259
6.33	FESEM images of 12 h UV-treated anodised titanium (series AR) in solutions of (A) pH 1 (B) pH 4 (C) pH 7 and (D) pH 11 after soaking in SBF for 7 days with UV irradiation	260

6.34	FESEM images of UV-treated anodised titanium (series AR) in solution of pH 1 with (A) 4 hours (B) 8 hours and (C) 12 hours after soaking in SBF for 7 days without UV irradiation	261
6.35	FIB micrographs of the cross sectional images for 12 h UV-treated anodised titanium (series AR) in solution of pH 1 after soaking in SBF for 7 days with UV irradiation	262
6.36	FIB micrographs of the cross sectional images for 12 h UV-treated anodised titanium (series AR) in solution of pH 4 after soaking in SBF for 7 days with UV irradiation	262
6.37	FIB micrographs of the cross sectional images for 12 h UV-treated anodised titanium (series AR) in solution of pH 7 after soaking in SBF for 7 days with UV irradiation	263
6.38	FIB micrographs of the cross sectional images for 12 h UV-treated anodised titanium (series AR) in solution of pH 11 after soaking in SBF for 7 days with UV irradiation	263
6.39	GAXRD patterns of 12 h UV-treated anodised titanium (series A) in solutions of (A) pH 1 (B) pH 4 (C) pH 7 and (D) pH 11 after soaking in SBF for 7 days with UV irradiation	265
6.40	GAXRD patterns of 12 h UV-treated anodised titanium (series AR) in solutions of (A) pH 1 (B) pH 4 (C) pH 7 and (D) pH 11 after soaking in SBF for 7 days with UV irradiation	266
6.41	FESEM images of anodised titanium after soaking in SBF for 7 days under different UV irradiation conditions	269
6.42	GAXRD patterns of anodised titanium after soaking in SBF for 7 days under different UV irradiation conditions	270
6.43	Schematic diagram of mechanism for bone-like apatite formation on anodised titanium under different UV irradiation conditions after soaking in SBF for 7 days	271
6.44	Surface morphologies of anodised titanium (A) before soaking in SBF; and after soaking in SBF under UV	274

	irradiation for (B) 1 day; (C) 2 days; (D) 3 days; (E) 4 days; (F) 5 days; (G) 6 days; and (H) 7 days	
6.45	Mechanism of the preferred and non-preferred nucleation site for growth of bone-like apatite	275
6.46	FTIR spectra of anodised titanium after soaking in SBF under UV irradiation (a) 1 day; (b) 2 days; (c) 3 days; (d) 4 days; (e) 5 days; (f) 6 days; and (g) 7 days.	276
6.47	Schematic of bone-like apatite formation in SBF under UV irradiation	278
7.1	Colourisation of anodised titanium obtained at 350 V and 70 mA.cm^{-2} for 10 minutes at various volume fraction of 1 M H_2SO_4 (12.5-50 vol %)	281
7.2	Surface morphology of anodised titanium obtained at 350 V and 70 mA.cm^{-2} for 10 minutes at various volume fraction of 1 M H_2SO_4 (12.5-50 vol %)	285
7.3	Surface mineralogy of anodised titanium obtained at 350 V and 70 mA.cm^{-2} for 10 minutes at various volume fraction of 1 M H_2SO_4 (12.5-50 vol %)	286
7.4	Surface topography of anodised titanium obtained at 350 V and 70 mA.cm^{-2} for 10 minutes at various volume fraction of 1 M H_2SO_4 (12.5-50 vol %)	286
7.5	FTIR spectra of anodised titanium obtained at 350 V and 70 mA.cm^{-2} for 10 minutes at various volume fraction of 1 M H_2SO_4 (12.5-50 vol %).	287
7.6	Water contact angle images of anodised titanium obtained at 350 V and 70 mA.cm^{-2} for 10 minutes at various volume fraction of 1 M H_2SO_4 (12.5-50 vol %)	289
7.7	Surface morphology of anodised titanium obtained at 350 V and 70 mA.cm^{-2} for 10 minutes at various volume fraction of 1 M H_2SO_4 (12.5-50 vol %) after soaking in SBF for 7 days	291
7.8	GAXRD patterns of anodised titanium obtained at 350 V and 70 mA.cm^{-2} for 10 minutes at various volume	292

	fraction of 1 M H_2SO_4 (12.5-50 vol %) after soaking in SBF for 7 days	
7.9	Colourisation of anodised titanium obtained at 350 V and 70 mA.cm^{-2} for 10 minutes at various volume fraction of 1 M H_2O_2 (12.5-50 vol %)	293
7.10	Surface morphology of anodised titanium obtained at 350 V and 70 mA.cm^{-2} for 10 minutes at various volume fraction of 1 M H_2O_2 (12.5-50 vol %)	295
7.11	Surface mineralogy of anodised titanium obtained at 350 V and 70 mA.cm^{-2} for 10 minutes at various volume fraction of 1 M H_2O_2 (12.5-50 vol %)	296
7.12	Surface topography of anodised titanium obtained at 350 V and 70 mA.cm^{-2} for 10 minutes at various volume fraction of 1 M H_2O_2 (12.5-50 vol %)	297
7.13	FTIR spectra of anodised titanium obtained at 350 V and 70 mA.cm^{-2} for 10 minutes at various volume fraction of 1 M H_2O_2 (12.5-50 vol %)	298
7.14	Water contact angle images of anodised titanium obtained at 350 V and 70 mA.cm^{-2} for 10 minutes at various volume fraction of 1 M H_2O_2 (12.5-50 vol %)	300
7.15	Surface morphology of anodised titanium obtained at 350 V and 70 mA.cm^{-2} for 10 minutes at various volume fraction of 1 M H_2O_2 (12.5-50 vol %) after soaking in SBF for 7 days	301
7.16	GAXRD patterns of anodised titanium obtained at 350 V and 70 mA.cm^{-2} for 10 minutes at various volume fraction of 1 M H_2O_2 (12.5-50 vol %) after soaking in SBF for 7 days	302
7.17	Colourisation of anodised titanium obtained at 350 V and 70 mA.cm^{-2} for 10 minutes at various volume fraction of 1 M $C_2H_4O_2$ (12.5-50 vol %)	303

7.18	Surface morphology of anodised titanium obtained at 350 V and 70 mA.cm^{-2} for 10 minutes at various volume fraction of 1 M $C_2H_4O_2$ (12.5-50 vol %)	306
7.19	Surface mineralogy of anodised titanium obtained at 350 V and 70 mA.cm^{-2} for 10 minutes at various volume fraction of 1 M $C_2H_4O_2$ (12.5-50 vol %)	307
7.20	Surface topography of anodised titanium obtained at 350 V and 70 mA.cm^{-2} for 10 minutes at various volume fraction of 1 M $C_2H_4O_2$ (12.5-50 vol %)	308
7.21	FTIR spectra of anodised titanium obtained at 350 V and 70 mA.cm^{-2} for 10 minutes at various volume fraction of 1 M $C_2H_4O_2$ (12.5-50 vol %)	309
7.22	Water contact angle images of anodised titanium obtained at 350 V and 70 mA.cm^{-2} for 10 minutes at various volume fraction of 1 M $C_2H_4O_2$ (12.5-50 vol %)	310
7.23	Surface morphology of anodised titanium obtained at 350 V and 70 mA.cm^{-2} for 10 minutes at various volume fraction of 1 M $C_2H_4O_2$ (12.5-50 vol %) after soaking in SBF for 7 days	312
7.24	GAXRD patterns of anodised titanium obtained at 350 V and 70 mA.cm^{-2} for 10 minutes at various volume fraction of 1 M $C_2H_4O_2$ (12.5-50 vol %) after soaking in SBF for 7 days	313
7.25	Colourisation of anodised titanium obtained at 350 V and 70 mA.cm^{-2} for 10 minutes at various volume fraction of 1 M NaOH (12.5-50 vol %)	314
7.26	Surface morphology of anodised titanium obtained at 350 V and 70 mA.cm^{-2} for 10 minutes at various volume fraction of 1 M NaOH (12.5-50 vol %)	317
7.27	Surface mineralogy of anodised titanium obtained at 350 V and 70 mA.cm^{-2} for 10 minutes at various volume fraction of 1 M NaOH (12.5-50 vol %)	318

7.28	Surface topography of anodised titanium obtained at 350 V and 70 mA.cm^{-2} for 10 minutes at various volume fraction of 1 M NaOH (12.5-50 vol %)	319
7.29	FTIR spectra of anodised titanium obtained at 350 V and 70 mA.cm^{-2} for 10 minutes at various volume fraction of 1 M NaOH (12.5-50 vol %)	320
7.30	Water contact angle images of anodised titanium obtained at 350 V and 70 mA.cm^{-2} for 10 minutes at various volume fraction of 1 M NaOH (12.5-50 vol %)	321
7.31	Surface morphology of anodised titanium obtained at 350 V and 70 mA.cm^{-2} for 10 minutes at various volume fraction of 1 M NaOH (12.5-50 vol %) after soaking in SBF for 7 days	323
7.32	GAXRD patterns of anodised titanium obtained at 350 V and 70 mA.cm^{-2} for 10 minutes at various volume fraction of 1 M NaOH (12.5-50 vol %) after soaking in SBF for 7 days	324

LIST OF SYMBOLS AND ABBREVIATIONS

•OH	-	Hydroxyl group
AFM	-	Atomic force microscopy
$C_2H_4O_2$	-	Acetic acid
CA	-	Calcium acetate monohydrate
$Ca_2O_7P_2$	-	Calcium diphosphate
$Ca_3O_8P_2$	-	Tricalcium phosphate
Ca-P	-	Calcium Phosphate
$CaTiO_3$	-	Calcium titanate
Cp-Ti	-	Commercially pure titanium
DSLR	-	Digital single-lens reflex camera
FESEM	-	Field emission scanning electron microscope
FIB	-	Focused ion beam
FTIR	-	Fourier transform infrared spectroscopy
GAXRD	-	Glancing angle X-ray diffraction
h	-	hour
H_2O_2	-	Hydrogen peroxide
H_2SO_4	-	Sulphuric acid
HAp	-	Hydroxyapatite
HCL	-	Hydrochloric acid
JCPDS	-	Joint Committee on Powder Diffraction Standards
$Na_2Ti_3O_7$	-	Sodium titanate
NaOH	-	Sodium hydroxide
SBF	-	Simulated body fluid
Ti	-	Titanium
TiO_2	-	Titanium dioxide
UV	-	Ultraviolet

UVA	-	Ultraviolet light type C
UVC	-	Ultraviolet light type A
β-GP	-	Beta-glycerophosphate disodium salt pentahydrate

CHAPTER 1

INTRODUCTION

1.1 Background

Titanium and its alloys are the most popular implant material due to its superior properties such as biocompatibility, good mechanical properties, low modulus of elasticity, and high corrosion resistance compared to other metals (Liu *et al*., 2004; Geetha *et al*., 2009 & Mohammad *et al*., 2012). There has been increased use of titanium, particularly as dental implants, cochlear replacements, screws for orthodontic surgery, bone fixation, artificial heart valves, and surgical instruments (Patel & Gohil, 2012). Figures 1.1 and 1.2 show the applications of titanium within the biomedical industry. However, titanium is a bio-inert material and does not allow significant bone apposition after implantation (Mohammad *et al*., 2012). The formation of a thin and passive titanium dioxide (TiO_2) layer occurs upon exposure of titanium to atmospheric conditions (Park *et al*., 2013).

TiO_2 is the most popular photocatalytic material due to its outstanding properties such as low cost, high stability, high photocatalytic performance, and strong oxidation ability (Augugliaro *et al*., 2010). Titanium dioxide (TiO_2) exists as three main crystalline phases, namely anatase, brookite, and rutile, of which rutile is the most common and stable form (Diebold, 2013). The band gaps for anatase and rutile TiO_2 are 3.20 eV and 3.02 eV, respectively (Hanaor & Sorrell, 2011). Hence, a number of research had been conducted on photocatalytic performance of TiO_2 due

to its wider band gap energy. Most research has been conducted on the photocatalytic properties of anatase and rutile TiO_2 compared to those on brookite TiO_2 (Diebold, 2013 & Koelsch *et al*., 2004).

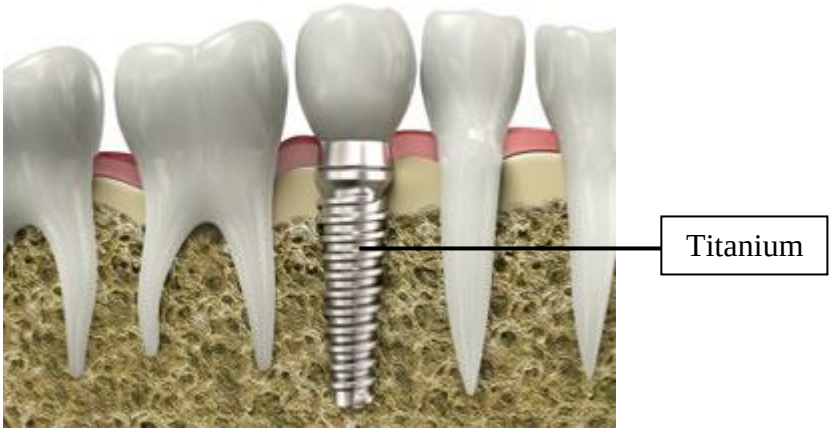

Figure 1.1: Artificial bone screw (Liu *et al*., 2004).

Figure 1.2: Artificial hip joint (Liu *et al*., 2004).

The surface of the implant plays a crucial role in promoting osseointegration. Osseointegration is important to ensure the implants integrated into bone for long-term successful clinical outcome. Properties such as porous, rough, high crystallinity, and high hydrophilicity are ideal to enhance the osseointegration process (Elias, 2010; Ehrenfest *et al*, 2010 & Kim *et al*., 2012). A number of efforts have been undertaken using anodic oxidation, alkaline treatment, gel oxidation, and plasma spraying in order to enhance the bioactivity of the titanium (Liu *et al.*, 2010). Among these, anodic oxidation is the simplest and cost-effective method. The anodic oxidation of

titanium is categorised by solid state diffusion in the oxide and/or by dissolution deposition in the electrolyte. Anodic oxidation combines electric field-driven metal and oxygen ion diffusion to form an oxide layer on the anode surface (Liu *et al*., 2004; Kim & Ramaswamy, 2009). This process thus enhances the adhesion and bonding, improves crystallinity, and increases the corrosion resistance of the inherent oxide layer (Liu *et al*., 2004). Post implantation, anodised titanium forms a bone-like apatite layer on the surface that bonds to living bone tissue. The composition and structure of bone-like apatite that is formed is very similar to human bone (Kasuga *et al*., 2002).

In this study, a mixture of β-glycerophosphate disodium salt pentahydrate and calcium acetate monohydrate (β-GP + CA) was used as the electrolyte. For biomedical applications, this solution provides phosphorous and calcium ions that promote bone tissue growth and thereby enhance the anchorage of the implant to the bone (Lee *et al*., 2015a & Abdullah *et al*., 2014). The *in vitro* bioactivities of the implant are normally evaluated by using simulated body fluid (SBF). The SBF solution is prepared by following the recipe of Kokubo & Takadama (2006) in order to study the precipitation of bone-like apatite as well as prediction of natural bone growth on the implant.

This study investigates the effect of processing parameters such as applied voltage, current density, anodising time, electrolyte concentration, stirring methods during anodic oxidation, bath temperature, UV light treatment condition and type of additive in electrolyte to improve the biocompatibility of the material as well as to improve the bonding time and reduce the healing time once the material is placed in the body.

1.2 Problem Statements

To date, anodic oxidation of titanium with a mixture of β-GP + CA requires a longer time (more that 300 days) to form bone-like apatite on the surface. This is due to the lack of sufficient nucleation sites on the oxide layer (TiO_2) for the growth of bone-like apatite (Abdullah, 2010). Using a mixture of β-GP + CA as the electrolyte for

preparing anodised titanium, Ishizama and Ogino (1995) observed that bone-like apatite was not formed on the surface of anodised titanium even after soaking in SBF for 300 days. Han *et al*. (2008) also noted the absence of bone-like apatite on the surface of anodised titanium after soaking in SBF for 90 days, and similar results were observed by Huang *et al*. (2007) and Abdullah (2010) after soaking in SBF for 50 days and 7 days, respectively.

In order to address the issues, this research was conducted to explore the effective ways to shorten the time for the growth of bone-like apatite on the surface of anodised titanium and improve the biocompatibility of the titanium. The tendency of the oxide layer to may exhibit bone-like apatite forming ability could be enhanced upon exposure to ultraviolet (UV) irradiation (Han *et al.*, 2008). Therefore, UV light treatment after anodic oxidation and UV irradiation during *in vitro* testing were conducted to elucidate the effect of UV irradiation on the bone-like apatite forming ability. Apart from that, additives such as sulphuric acid (H_2SO_4), hydrogen peroxide (H_2O_2), acetic acid ($C_2H_4O_2$) and sodium hydroxide (NaOH) were used in order to activate the nucleation sites of bone-like apatite.

1.3 Objectives

The present research has the following objectives:

(a) To investigate the anodic oxidation behaviour of titanium surface in a weak organic acid mixture (β-glycerophosphate + calcium acetate).

(b) To propose and access a new approach of *in vitro* bioactivation of the anodised titanium in SBF with UV irradiation.

(c) To explore the effect of stirring methods and bath temperature during anodic oxidation on the surface properties of anodised titanium.

(d) To investigate the effect of UV light treatment after anodic oxidation on the bone-like apatite forming ability of the anodised titanium.

(e) To characterise the growth of bone-like apatite on the surface of anodised titanium in SBF.

(f) To investigate the effect of additives in mixture of β-GP + CA electrolyte on the bone-like apatite forming ability of anodised titanium.

1.4 Scope of Study

The scope of this study is as follows:

(a) Oxide layers on titanium were produced via anodic oxidation in mixtures of β-GP + CA. The parameters used are as follow:

- Applied voltage : 50-350 V
- Current density : 10-70 mA/cm^2
- Anodising time : 5-10 min
- Concentration of β-GP + CA : 0.02 M + 0.2 M and 0.04 M +0.4 M
- Temperature : ~25°C

(b) SBF was used to conduct the *in vitro* testing by following Kokubo's recipe. *In vitro* testing were conducted in three different conditions:

- Without UV irradiation
- With short wavelength (254 nm) UV irradiation
- With long wavelength (365 nm) UV irradiation

(c) Different stirring methods and varying bath temperatures were used to investigate the effect of these parameters on the resultant surface properties of the anodised titanium. The parameters used are as follows:

- Stirring Method : Magnetic, Ultrasonic, Water Bath
- Agitation speed : 300-1500 rpm
- Ultrasonic amplitude : 20-60 μm
- Bath temperature : 4-100°C

(d) UV light treatment was conducted after anodic oxidation. The parameters used for UV light treatment are as follows:

- pH of solution during UV light treatment : 1-11
  **pH of solution was adjusted using H_2SO_4 and NaOH
- Duration of UV light treatment : 4-12 hours
- Wavelength of UV irradiation : 365 nm

(e) UV-treated anodised titanium was soaked in SBF for 7 days. The samples were analysed each day in order to investigate the growth mechanism of bone-like apatite.

(f) Additives were added to the mixture of β-GP + CA electrolyte to explore

the effect on bone-like apatite forming ability of anodised titanium. Parameters in this part of the study are as follows:

- Types of additives : H_2SO_4, H_2O_2,$C_2H_4O_2$ and NaOH
- Molarity of additive : 1 M
- Volume fraction of additives : 12.5-50.0 vol %

(g) The characterisation of anodised titanium were carried out using the following techniques:

- Digital camera - colourisation
- Colourimeter - colourisation
- Field emission scanning electron microscopy (FESEM) - surface morphology
- Focus ion beam (FIB) - cross sectional image
- Glancing angle X-ray diffractometer (GAXRD) - surface mineralogy
- Laser Raman microspectroscopy - surface mineralogy
- Atomic force microscopy (AFM) - surface topography
- Fourier transform infrared spectroscopy (FTIR) - structural characteristic
- Goniometer - surface wettability and surface energy
- UV-VIS spectroscopy - optical properties

1.5 Significance of Study

This section briefly describes the significances of this project with regard to helping in faster recover from injury and aging, and surface modification technology of the biomedical implant.

(a) Injury and aging

Kovan (2008) reported that the most common causes for bone fracture are vehicles accident, severe assault and falls. Meanwhile, Farr & Khosla (2016) claimed that aging is the most significant risk factor for osteoporosis and fractures. This research can assist in helping in the growth of new bone on the implant surface and help the patients experienced bone fracture caused by

accident and osteoporosis to replace fractured bone. Anodisation of titanium in mixture of calcium acetate and β-glycerophosphate will enhance the osseointegration of tissues and bones with the implant titanium and shorten the recovery time of patient suffered injury.

(b) Surface medication technology

This research can show the potential of anodised titanium for biomedical uses. Furthermore, the new approach of *in vitro* testing under UV irradiation on anodised titanium can provide information on the effect of UV irradiation during immersion in SBF.

1.6 Novelty of study

The present work reveals novel methods (UV irradiation and additives addition in β-GP + CA) to enhance the rate of growth of bone-like apatite on the surface of titanium metal anodised in a mixture of β-GP + CA.

Previous researchers (Ishizama & Ogino, 1995; Huang *et al*., 2007) observed absent of bone-like apatite on anodised surface even after soaking in SBF for more than 300 days. Han *et al*. (2008) and Gao *et al*. (2013) proved that UV irradiation is able to enhance the bioactivity of anodic films. However, better understanding of the effect of UV irradiation on growth of bone-like apatite need to be elucidated due to absent of studies on investigating the effect of UV irradiation during *in vitro* testing.

Therefore, the study was carried out was also able contribute new knowledge in biomaterials research field and propose novel methods to accelerate the growth of bone-like apatite. In this study, highly crystallised bone-like apatite was fully covered on the anodised surface after soaking in SBF with UV irradiation for 7 days.

Moreover, there are no available study and literature with regards to effect of additives addition in β-GP + CA electrolyte on bone-like apatite forming ability of anodised titanium. In this study, H_2SO_4, H_2O_2, $C_2H_4O_2$ and NaOH were added in mixture of β-GP + CA. It was found that addition of additives in β-GP + CA electrolyte is capable to accelerate the formation of highly crystallised bone-like apatite on anodised surface in 7 days only.

CHAPTER 2

LITERATURE REVIEW

2.1 Introduction

Titanium and its alloys have been widely used in biomedical applications as implant materials due to its good biocompatibility with hard tissue. However, titanium and its alloys do not facilitate osseointegration since the surface of machined titanium is smooth, low in crystallinity, hydrophobic, and poor in bioactivity. Consequently, machined implants do not promote significant better bone apposition (Liu *et al*., 2004). Therefore, it is necessary to conduct surface modification though anodic oxidation in order to produce micro-rough, highly crystalline, hydrophilic, and bioactive surfaces. This particular mechanism will enhance the process of osseointegration. Anodic oxidation is a simple and low-cost surface modification method for titanium-based implants and has been widely used for dental implants and medical fastener (Kim & Ramaswamy, 2009). *In vitro* and *in vivo* tests proved that anodised titanium implants showed a considerable improvement in their osseointegration capability as compared to the machined titanium implants (Kim & Ramaswamy, 2009).

2.2 Biomaterials

2.2.1 Overview of Biomaterials

Biomaterials can be defined as "*any substance (other than a drug) or combination of substances, synthetic or natural in origin, which can be used for any period of time, as a whole or as a part of a system which treats, augments, or replace any tissue, organ, or function of the body*" (Boretos & Eden, 1984).

Biomaterials in the form of implants are widely used to replace, repair and restore the damaged organs or tissues and thus improve the life quality of the patient. For blood contact applications, biomaterials are inserted into blood vessels or devices that are permanently implanted to remove and return the blood from the body. For soft tissue applications, biomaterials are implanted to augment or redefine the damaged tissue. On the other hand, for orthopaedic and dental applications, biomaterials are implanted to repair the defective parts of the body (Nascimento *et al*., 2007). Figure 2.1 presents the human anatomy and organs where biomedical materials are used. Biomaterials are very important for improving the quality and longevity of human life (Manivasagam *et al*., 2010).

Basically, biomaterials can be divided into three categories which are metals, ceramics and polymers. Each biomaterials has its own unique functions whether for hard or soft tissue implants. The selection of biomaterials is important in order to provide true biological and mechanical match for living tissue. Table 2.1 shows the comparison among metals, ceramics and polymers biomaterials. Table 2.2 shows the biomedical application of metals, ceramics and polymers biomaterials (Bauer, 2013).

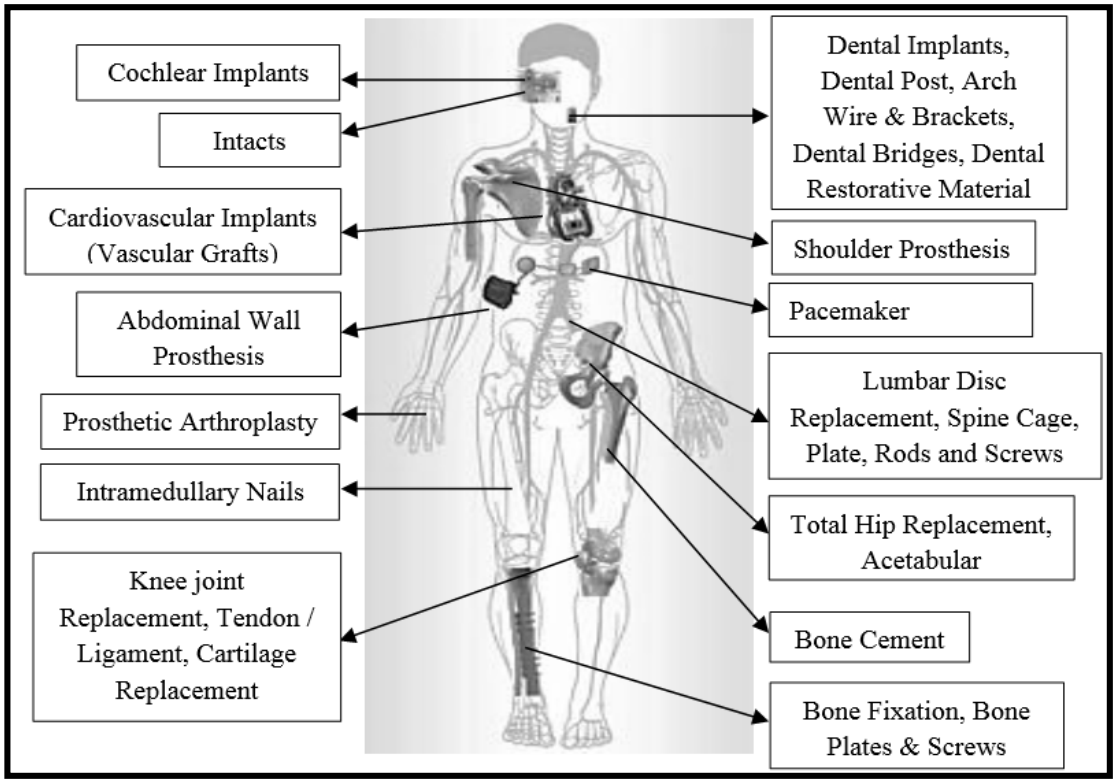

Figure 2.1: Implants in the human body (Patel & Gohil, 2012).

Table 2.1: Advantages and disadvantages of metals, ceramics and polymers for biomedical applications (Nallaswamy, 2008)

Materials	**Advantages**	**Disadvantages**
Metals	High strength, high ductility biocompatibility,	Low corrosion resistance, may disrupt the interfacial attachment.
Ceramics	Biocompatibility, minimal thermal and electrical conductivity; modulus of expansion, colour and chemical composition are similar to bone.	Low mechanical, tensile and shear strength under fatigue loading, low attachment strengths for some coatings with the substrate interface.
Polymers	Low term experience, biocompatibility, ability to control properties through compositional means	Porous polymers undergo elastic deformation and lead to closing and opening of regions intended for tissue growth, difficult to clean contaminations

Table 2.2: Example of metal, ceramic, and polymer biomaterial use for biomedical applications (Bauer, 2013)

No	Material	Medical applications
	Metals	
1	Cobalt – chromium alloys	Artificial heart valves, dental prosthesis, orthopaedic fixation plates, artificial joint components, vascular stents
2	Stainless steel	Dental prostheses, orthopaedic fixation plates, vascular stents
3	Titanium alloys	Artificial heart valves, dental implants, artificial joint components, orthopaedic screws, pacemaker cases, vascular stents
4	Gold or platinum	Dental fillings, electrodes for cochlear implants
5	Silver–tin–copper alloys	Dental amalgams
	Ceramics	
6	Aluminium oxides	Orthopaedic joint replacement, orthopaedic load-bearing implants, implant coatings, dental implants
7	Zirconium oxides	Orthopaedic joint replacement, dental implants
8	Calcium phosphates	Orthopaedic and dental implant coatings, dental implant materials, bone graft substitute materials
9	Bioactive glasses	Orthopaedic and dental implant coatings, dental implants, facial reconstruction components, bone graft substitute materials, bone cements
	Polymers	
10	Polyethylene	Orthopaedic joint implants, syringes
11	Polypropylene	Heart valves, sutures, syringes
12	Polydimethylsiloxane	Breast implants, contact lenses, knuckle replacements, heart valves, artificial hearts
13	Polyethyleneterephthalate	Vascular grafts, sutures, blood vessels
14	Polyethyleneglycol	Pharmaceutical fillers, wound dressings
15	Polytetafluoroethylene	Vascular grafts, sutures
16	Collagen	Orthopaedic repair matrices, nerve repair matrices, tissue engineering matrices
17	Hyaluronic acid	Orthopaedic repair matrices
18	Elastin	Skin repair matrices
19	Fibri	Haemostatic products, tissue sealants
20	Chitosan	Wound dressing
21	Alginate	Wound dressing

2.2.2 Important Properties of Biomaterials for Implants

The biomaterials used for implant must possess important properties such as biocompatibility, good mechanical properties, and non-toxicity for a long term usage in human body without any negative effects. Table 2.3 briefly describes the important properties of biomaterials (Patel & Gohil, 2012).

Table 2.3: Important properties of biomaterials for use as implants (Patel & Gohil, 2012; Basu & Nath, 2009)

Properties	Brief Description
Host Response	Response of the host organism either local or systemic to the implanted material. There are 3 types of host response: a) *Bioinert / biotoletant* • Unable to induce any interfacial biological bond between implant and bone. • Examples: alumina, titanium and zirconia. b) *Bioactive* • Able to attach directly with body tissues and form chemical and biological bonds during early stages of the post implantation period. • Examples: 45S5 bioglass and calcium phosphates. c) *Bioresorbable* • Gradually resorbed before they finally disappear and are totally replaced by new tissue *in vivo*. • Examples: bone cement and tricalcium phosphate.
Biocompatibility	Ability of a material to perform without any adverse host response in a specific application implies harmony with the living system.
Biofunctionality	Ability to withstand load transmission and stress distribution, allowing for movement, controlling of fluid flow of blood, ability to provide space filling, electrical stimuli, light and sound transmission.
Functional Tissue Structure and Pathobiology	Ability to govern the structure of normal and abnormal cells, tissues and organs.
Non - toxicology	Toxicity of biomaterials will cause cell and human death
Sufficient Mechanical Properties	Biomaterials should possess high tensile strength, yield strength, elastic modulus, surface finish, creep, hardness and be easy to manufacture
High Corrosion Resistance	Avoid toxic ions
High Wear Resistance	Avoid implant loosening.

2.3 Metallic Implant Materials

2.3.1 Overview of Metallic Implant Materials

Metals had been used as implant materials for more than 100 years when Lane used metal plate to fix the bone fracture. However, metal implants suffer from corrosion and strength problems (Lane, 1895). In the 1920s, stainless steel was used for these applications (Hermawan *et al*., 2011). In 1932, cobalt-based alloys such as Vitallium were introduced for biomedical applications (Elias *et al*., 2008a). Titanium and its alloys were introduced in 1950s and a number of modification methods were applied to alter the alloy composition and surface properties in order to improve the functionality and implant duration in the human body (Geetha *et al*., 2009). Apart from that, biodegradable metals have been developed to meet the requirements of biomedical applications. Biodegradable metals permit the implants to degrade in biological environments. In term of mechanical properties, biodegradable metals are more suitable for internal bone fixation compared to the biodegradable polymers (Hermawan & Mantovani, 2009). Table 2.4 shows the examples of metallic biomaterials used for implants and their mechanical properties.

Table 2.4: Comparison of mechanical properties of commonly used metals and its alloys for biomedical applications (Hermawan *et al*., 2011; Nag & Banerjee, 2012)

Metallic Biomaterial	**Young's Modulus (GPa)**	**Yield Strength (MPa)**	**Ultimate Tensile Strength (MPa)**
Stainless Steel	200	170-750	465-950
Co-Cr-Mo	200-230	275-1585	600-1795
Commercially pure Ti	105	692	785
Ti-6A1-4V	110	850-900	960-970
Iron – annealed plate	200	150	210
Fe35Mn alloy, powder	N/A	235	550
Magnesium, annealed sheet	45	90	160
WE43 magnesium alloy, temper T6	44	170	220

2.3.2 Titanium and its Alloys

Titanium and its alloys were widely used as implant materials due to its high biocompatibility and high corrosion resistance. The Young's modulus of titanium and its alloys is only half of that of stainless steel or Co-Cr alloys. However, the properties of titanium are closer to cortical bones (Hanawa, 2008.). The applications of titanium and its alloys as implants includes cochlear replacements, bone and joint replacements, dental implants for tooth fixation, screw parts for orthodontic surgery, bone fixation like nails, screws and plates, artificial heart valves and surgical instruments (Patel & Gohil, 2012). Table 2.5 shows the mechanical properties of the titanium and its alloys for implants.

Table 2.5: Comparison of mechanical properties among titanium and its alloys (Long & Rack, 1998)

Alloy Designation	**Microstructure**	**Young's Modulus (GPa)**	**Yield Strength (MPa)**	**Ultimate Tensile Strength (MPa)**
Commercially pure Ti	α	105	692	785
Ti-6A1-4V	α/β	110	850-900	960-970
Ti-6Al-7Nb	α/β	105	921	1024
Ti-5Al-2.5Fe	α/β	110	914	1033
Ti-5Al-.5Fe	Metastable β	74-85	1000-1060	1060-1100
Ti-15Mo-5Zr-3Al	Metastable β	75	870-968	882-975
	Aged β + α	88-113	1087-1284	1099-1312
Ti-15Mo-2.8Nb-3Al	Metastable β	82	771	812
	Aged β + α	100	1215	1310
Ti-13Nb-13Zr	α/β	79	900	1030
Ti-15Mo-3Nb-0.3O (21SRx)	Metastable β + silicides	82	1020	1020
Ti-35Nb-7Zr-5Ta	Metastable β	55	530	590
Ti-35Nb-7Zr-5Ta-0.4O	Metastable β	66	976	1010

Among all the titanium and its alloys, commercially pure Ti and Ti-6Al-4V are the most commonly used materials for biomedical and implant applications. Although Ti-6Al-4V has high reputation for biocompatibility and corrosion

resistance, it can release ions such as aluminium (Al) and vanadium (V) which are toxic and can cause long term health problems such as Alzheimers disease, neuropathy, and ostemomalacia. These problems affect the long-term use of Ti-6Al-4V for implant applications (Geetha *et al*., 2009).

On the other hand, commercially pure titanium (Cp Ti) can be considered as the best biomaterial among titanium and its alloys owing to Cp Ti exhibiting the best biocompatible metallic surface. This is due to the build-up of a stable and inert oxide layer. Apart from that, Cp Ti also demonstrates good physical properties such as low level of electronic conductivity, high corrosion resistance, thermodynamic state at physiological pH value, low ion formation tendency in aqueous environments, and isoelectric point of the oxide of 5-6 (Elias *et al*., 2008a). Generally, Cp Ti can be classified into four types which are Cp Ti Grade 1, Cp Ti Grade 2, Cp Ti Grade 3 and Cp Ti Grade 4. Among all types of Cp Ti, Cp Ti Grade 4 has highest ultimate tensile strength and yield strength at 1.0% offset but lowest elongation. The mechanical properties for different types of Cp Ti are presented in Table 2.6.

Table 2.6: Mechanical properties of different grade of Cp Ti (ZAPP Materials Engineering, 2012)

Types of Cp Ti	**Ultimate Tensile Strength (MPa)**	**Yield Strength at 1.0% Offset (MPa)**	**Elongation (%)**
Cp Ti Grade 1	290-410	≥ 200	30
Cp Ti Grade 2	390-540	≥ 270	22
Cp Ti Grade 3	460-590	≥ 350	18
Cp Ti Grade 4	540-740	≥ 410	16

2.3.3 Properties of Titanium Implants

It is well known that titanium and its alloys are one of the popular biomaterials for implants application due to its properties such as biocompatibility, osseointegration, good mechanical properties, low modulus of elasticity, and high corrosion resistance. Nowadays, there is an increasing trend in using titanium implants especially for dental implants and prostheses (Özcan & Hämmerle, 2012). The important

properties of titanium and its alloy for biomedical application are presented in Table 2.7.

Table 2.7: Important properties of titanium in biomedical applications (Mohammed *et al*., 2012; Oldani & Dominguez, 2012; Ogawa & Nishimura, 2003; Sumner & Galante, 1992; Lilley *et al*., 1992)

Properties of titanium and its alloys	**Description**
Biocompatibility	• Cp TI, α + β and β type • Non-toxic • Hydrated titanium oxide enhanced the growth of calcium phosphorous compounds and accelerated the osseointegration
Osseointegration	• Able to integrate well with adjacent bone • Success rate ≈ 65 %
Mechanical Properties	• Able to withstand a variety of loads during physical activities • High strength, high ductility, high fracture toughness, crack resistance, high bending strength, high fatigue resistance, and admission strain (the ratio of yield strength to modulus of elasticity. • Suitable for load bearing or non-load bearing applications.
Low Modulus of Elasticity	• Not very high of compared to human bone • Adequate mechanical stress on the adjacent bone can be avoided due to the low modulus of elasticity. • Reduce the probability of bone cells damage
Corrosion Resistance	• Protective TiO_2 surface layer

2.3.4 Application of Titanium and its Alloy in Biomedical Industry

Titanium and titanium alloys are widely used in biomedical devices and components, especially as hard tissue replacements and for cardiac and cardiovascular applications. Figures 2.2 to Figure 2.5 show the applications of titanium and its alloys in biomedical applications.

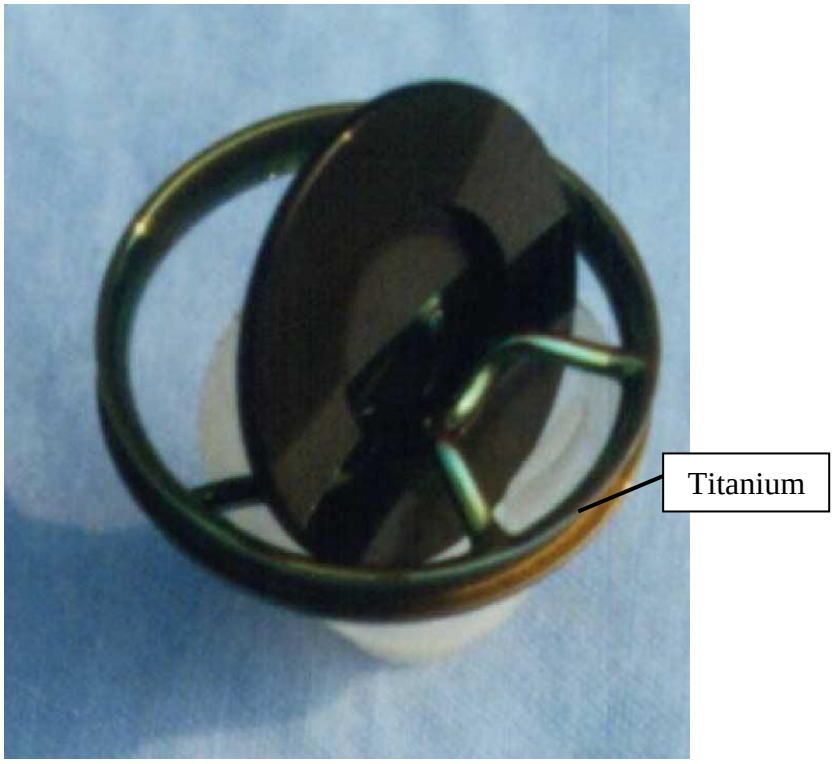

Figure 2.2: Artificial heart value (Liu *et al*., 2014).

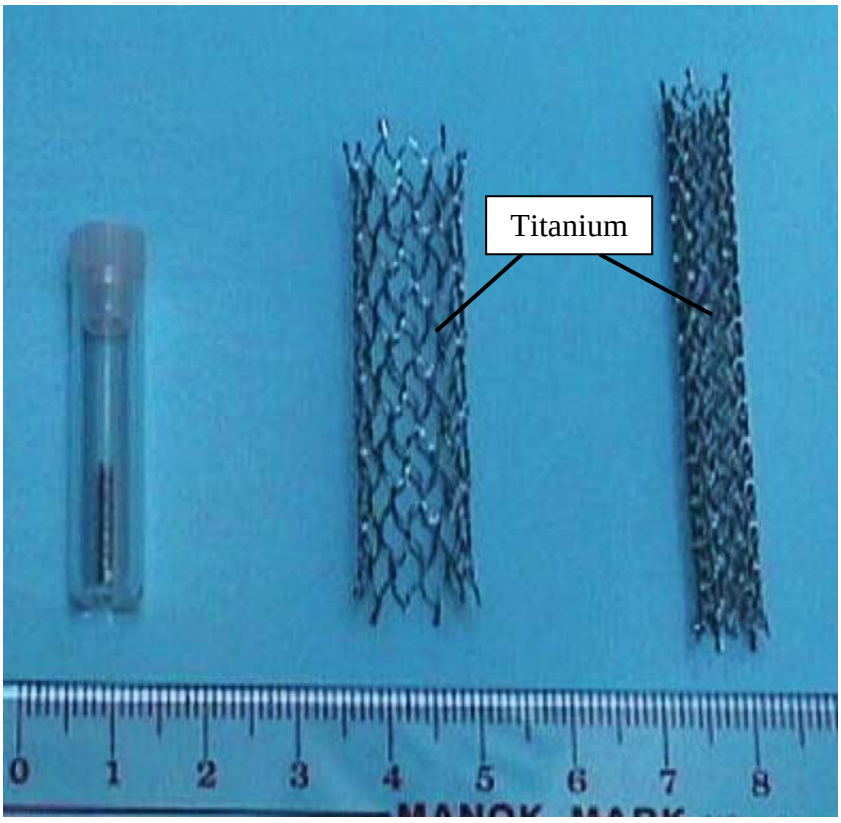

Figure 2.3: Artificial vascular stents (Liu *et al*., 2014).

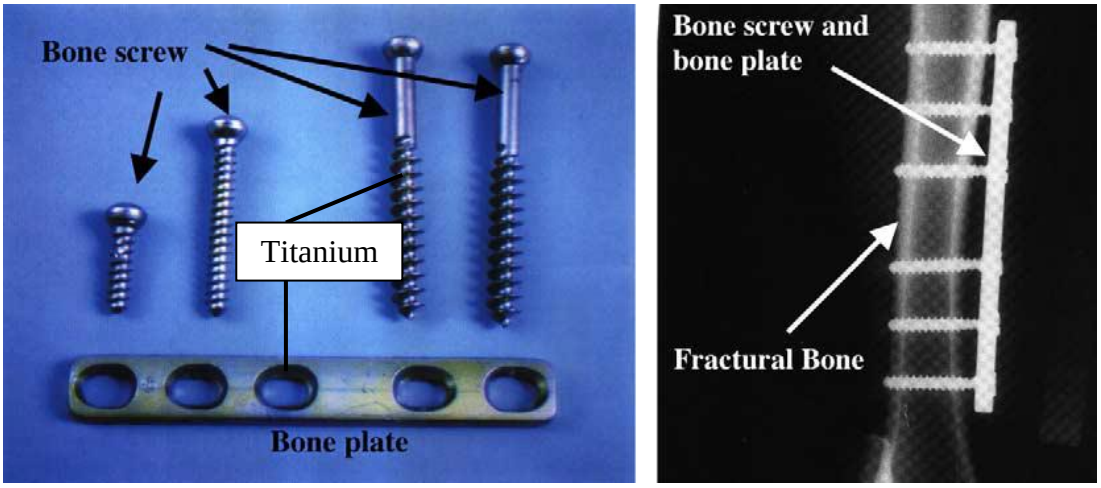

Figure 2.4: Bone screw and bone plate (Liu *et al*., 2014).

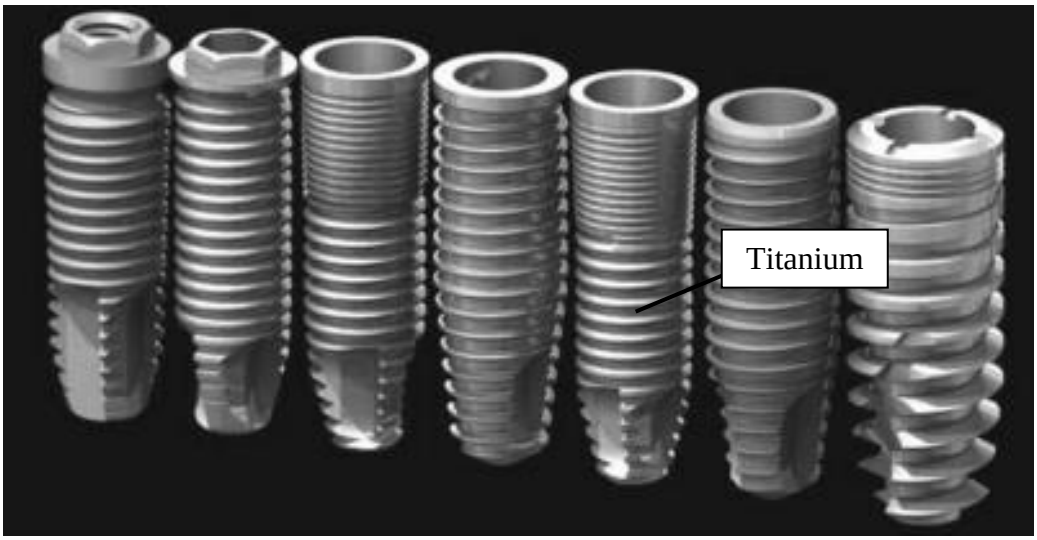

Figure 2.5: Commercial dental implant (Elias *et al*., 2008a).

2.4 Titanium Dioxide

2.4.1 Overview of Titanium Dioxide

Titanium is an oxide of titanium and is also known as titanium (IV) oxide, titania, titanium white, E171 in food colouring and pigment white 6 in building paints. The photocatalytic property of TiO_2 was first discovered when used as a white pigment in buildings since the pigment bleached under solar irradiation. Since then TiO_2 has been widely used in many industrial applications (Lan *et al.*, 2013).

2.4.2 Polymorphs of Titanium Dioxide

The oxide layer on titanium is a passive film and normally made up of two forms: amorphous or low crystalline stoichiometric TiO_2. Titanium dioxide has three naturally occurring crystallographic forms which are anatase, brookite and rutile. Rutile is the most common and stable form and only anatase and rutile are manufactured on a large scale.

Rutile structure consists of a slightly distorted hexagonal close packing of oxygen atoms with the titanium atoms occupying half of the octahedral interstices. On the other hand, anatase and brookite are both based on cubic packing of the oxygen atoms with octahedral coordination (Rouquerol *et al*., 2013). It is reported that anatase is the most active, rutile is less active, and brookite is not active at all for photocatalytic applications (Liu, 2012). Anatase TiO_2 is generally accepted to be a better photocatalyst than rutile and brookite. However, rutile TiO_2 is the most thermodynamically stable phase among all the titanium dioxide forms (Mantz, 2010). Figures 2.6 to 2.8 demonstrate the crystal lattice structures of rutile, anatase, and brookite TiO_2. Table 2.8 compares the properties between rutile, anatase, and brookite forms of TiO_2.

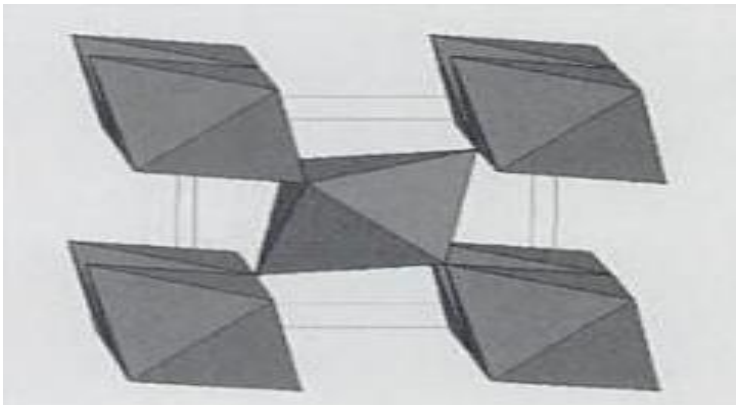

Figure 2.6: Structure of rutile TiO_2 (Winkler, 2003).

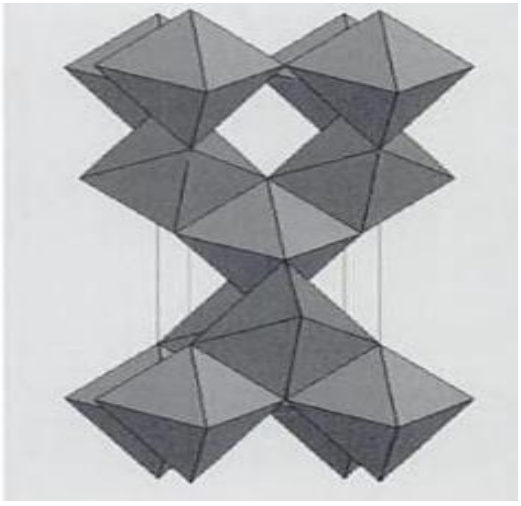

Figure 2.7: Structure of anatase TiO_2 (Winkler, 2003).

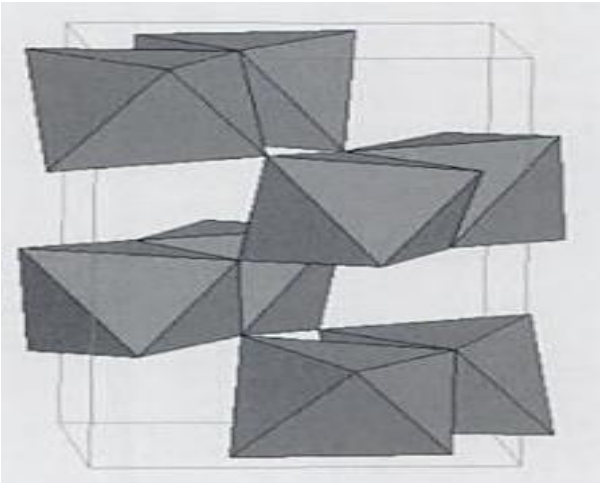

Figure 2.8: Structure of brookite TiO_2 (Winkler, 2003).

Table 2.8: Properties of rutile, anatase, and brookite TiO_2 (Winkler, 2003)

Properties	**Rutile TiO_2**	**Anatase TiO_2**	**Brookite TiO_2**
Density (g/cm^3)	4.2 – 4.3	3.8 – 3.9	3.9 – 4.1
Point group according to Schonflies	D_{4h}	D_{4h}	D_{2h}
a (nm)	0.4594	0.3785	0.9184
b(nm)	0.4594	0.3785	0.5447
c (nm)	0.2958	0.9514	0.5245
Volume of the elementary cell (nm^3)	62.07	136.25	257.38
Molar volume (cm^3/mol)	18.693	20.156	19.377
Moh's hardness	6.5 – 7	5.5 – 6.0	5.5 – 6.0
Melting point (^oC)	1830 – 1850	Transforms to rutile	Transforms to rutile

2.4.3 Photocatalytic Properties of Titanium Dioxide

The Singh (2008) defined photocatalysis as a process in which light is used to activate a substance, the photocatalyst, which modifies the rate of a chemical reaction without being involved itself in the chemical transformation. Photocatalysis can be classified as an advanced oxidation process. Photocatalysis in the presence of an irradiated semiconductor has proven to be effective in the field of environmental remediation. Semiconductors are superior photocatalyst due to it favourable combination of electronic structure, light absorption properties, charge transport characteristics, and long lifetimes. In fact, the irradiation of a semiconductor oxide with light will produce hydroxyl radicals on the catalyst surface (Augugliaro *et al.*, 2010).

Photocatalysts are widely used in common industrial applications such as photocatalytic water splitting, purification of pollutants, photocatalytic self-cleaning, photocatalytic antibacterial, photo-induced super hydrophilicity, and photosynthesis (Lan *et al.*, 2013). To date, researchers in the photocatalysis field have clarified the following advantages of photocatalysis (Kaneko & Okura, 2002).

(a) Multiple process such as reduction and oxidation, proceed successively in a one pot reaction

(b) Catalysts can be separated and reused easily

(c) The reactions proceed at ambient temperature under atmospheric pressure

(d) Unlike ordinary organic synthetic procedures, water can be used as a solvent and this enables the use of water-soluble organic substrates

(e) Sustainable and environmental friendly chemical processes

(f) Inexpensive

(g) Minimal infrastructural requirements

Semiconductors such as titanium oxide (TiO_2), zinc sulphide (ZnS), strontium titanate ($SrTiO_3$), zinc oxide (ZnO), zirconium dioxide (ZrO_2), cadmium sulphide (Cds), molybdenum disulfide (MoS_2), iron (III) oxide (Fe_2O_3), tungsten trioxide (WO_3), has been widely used as photocatalysts. In fact, the photocatalytic properties of the photocatalyst is strongly dependent on the band gap, energy level locations, mean life time, and mobility of electron and holes, light absorption coefficient, nature of the interface, as well as the method of preparation. Figure 2.9 shows the band gaps of different semiconductors (Augugliaro *et al*., 2010).

An ideal photocatalyst should present the following characteristics (Augugliaro *et al*., 2010):

(a) High reaction rate with wider band bad

(b) Photostability

(c) Chemical and biological inactivity

(d) Low cost

(e) Non-toxic and harmless

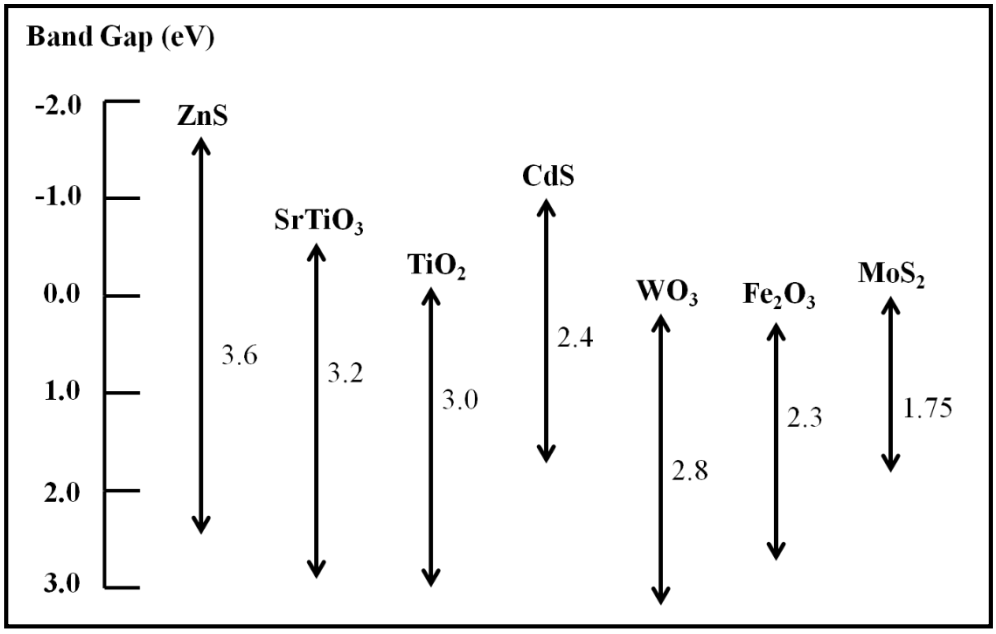

Figure 2.9: Band gap for commonly used photocatalysts (Augugliaro *et al*., 2010).

The photocatalyst will produce pairs of electrons and holes after it absorbs the UV irradiation from the sunlight or illuminated light source. The electrons in the valance band of the photocatalyst become energetic after irradiation by UV. The electron will be excited to the conduction band and thus creating negative electron (e^-) and positive hole (h^+) pairs. The electrons and holes can recombine and can release the absorbed heat without any chemical effects. The valance band hole is strongly oxidising. However, the conduction band electron is strongly reducing. The band gap is the energy difference between the valance band and conduction band. The positive hole of the photocatalyst can react with water molecules to form hydrogen gas and hydroxyl radicals (•OH). The •OH radicals are able to rapidly attack the pollutants at the solution surface. On the other hand, the negative electrons will react with the oxygen molecule and form superoxide anions (O_2^-). The process will continue as long as there is irradiation (Augugliaro *et al*., 2010 & Al-Rasheed, 2005). Figure 2.10 shows the simplified mechanism for the photocatalytic process of a semiconductor catalyst.

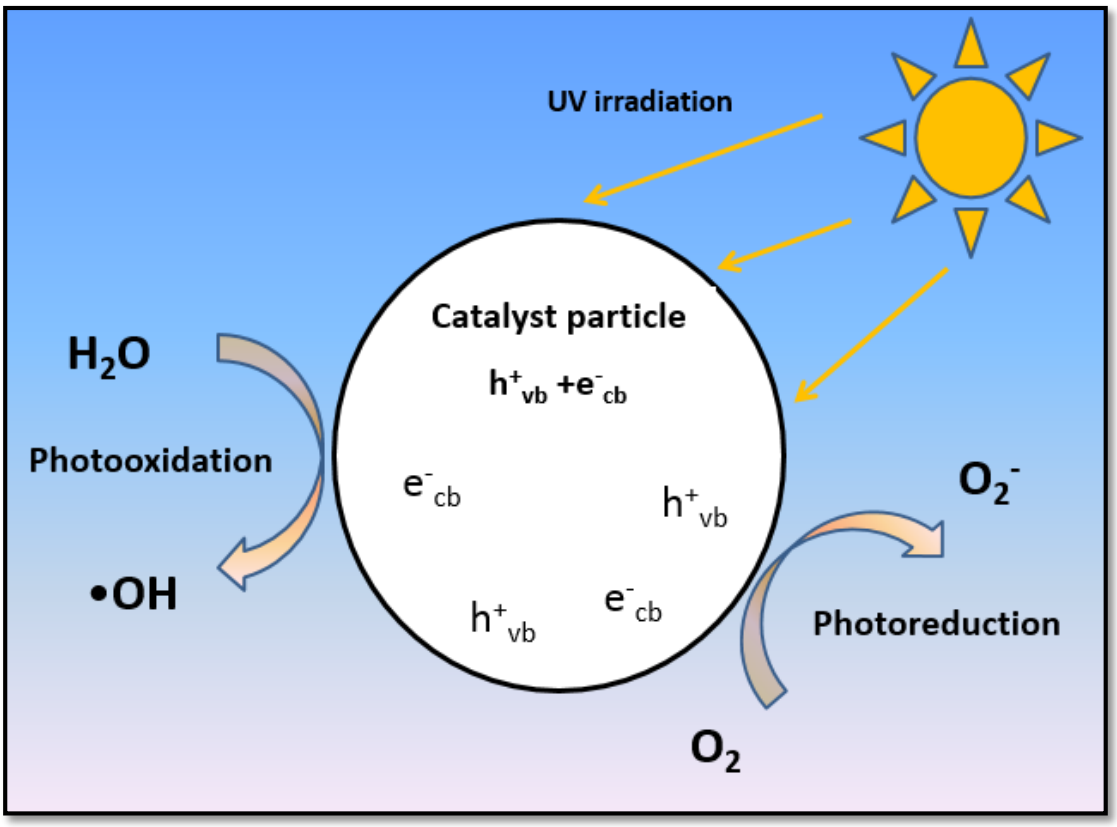

Figure 2.10: Mechanism of the photocatalytic process (re-illustrated from Al-Rasheed, 2005).

The equations 2.1 to 2.10 show chemical reactions that occur during the photocatalytic process at the TiO_2-water interface. Generally, •OH, $•O_2^-$ and H_2O_2 are the key reactive oxygen species (ROS) are formed during the photocatalytic process (Augugliaro *et al*., 2010 & Cai, 2013).

- TiO_2 reacts with UV light and produces pairs of free electrons ($e^-_{(CB)}$) and positively charged holes ($h^+_{(VB)}$) as shown in Equation 2.1.

  $TiO_2 + h\nu \rightarrow TiO_2 (e^-_{(CB)} + h^+_{(VB)})$ (2.1)

- Equation 2.2 and Equation 2.3 show the water molecular or hydroxide ions trapped in the positively charged hole and form the hydroxyl radicals (•OH)

  $H_2O + h^+_{(VB)} \rightarrow •OH + H^+$ (2.2)

  $OH^- + h^+_{(VB)} \rightarrow •OH$ (2.3)

- The Ti^{4+} reacts with the conduction band electron and is reduced to Ti^{3+} as shown in equation 2.4.

  $Ti^{4+} + e^-_{(CB)} \rightarrow Ti^{3+}$ (2.4)

REFERENCES

Abbasi, S., Golestani-Fard, F., Mirhosseini, S. M. M., Ziaee, a. & Mehrjoo, M. (2013). Effect of electrolyte concentration on microstructure and properties of micro arc oxidized hydroxyapatite/titania nanostructured composite. *Materials Science & Engineering. C, Materials for Biological Applications*, *33(5)*, pp. 2555-2561.

Abdullah, H .Z. & Sorrell, C. C. (2012). Titanium dioxide (TiO_2) films by anodic oxidation in phosphoric acid. *Advanced Materials Research*, *545*, pp. 223-228.

Abdullah, H. Z. & Sorrell, C. C. (2007a). TiO_2 thick films by anodic oxidation. *Journal of Australia Ceramic. Society, 43(2)*, pp. 125-130.

Abdullah, H. Z. & Sorrell, C. C. (2007b). Preparation and characterisation of TiO_2 thick films fabricated by anodic oxidation. *Material Science Forum*, *56*, pp. 2159-2162.

Abdullah, H. Z. (2010). *Titanium surface modification by oxidation for biomedical application*. University of New South Wales: Ph.D.'s Thesis.

Abdullah, H. Z., Koshy, P. & Sorrell, C. C. (2014). Anodic oxidation of titanium in mixture of β-glycerophosphate (β-GP) and calcium acetate (CA). *Key Engineering Materials*, *594*, pp. 270-280.

Abdullah, H. Z., Lee, T. C., Idris, M. I., & Sorrell, C. C. (2015). Effect of current density on anodised titanium in mixture of β-glycerophosphate (β-GP) and calcium acetate (CA). *Advanced Materials Research*, *1087*, pp. 212-217.

Aguilar, F., Charrondiere, U. R., Dusemund, B., Galtier, P., Gilbert, J., Gott, D. M., Grilli, S., Guertler, R., Kass, G. E. N., Koenig, J., Lambré, C., Larsen, J. C.,

Leblanc, J. C., Mortensen, A., Parent-Massin, D., Pratt, I., Rietjens, I., Stankovic, I., Tobback, P., Verguieva, T. & Woutersen, R. (2009). Scientific opinion of the panel on food additives and nutrient sources added to food on calcium acetate, calcium pyruvate, calcium succinate, magnesium pyruvate magnesium succinate and potassium malate added for nutritional purposes to food supplements following a request from the european commission. *The EFSA Journal, 1088,* pp.1-25.

Ahmed, W., Ali, N. & Oechsner, A. (2008). *Biomaterials and biomedical engineering.* Dürnten: Trans Tech Publication.

Albers, G. M., Tomkiewicz, R. P., May, M. K., Ramirez, O. E. & Rubin, B. K (1996). Ring distraction technique for measuring surface tension of sputum: relationship to sputum clearability. *Journal of Applied Physiology, 81(6),* pp. 2690-2695.

Albrektsson, T., Branemark, P. I., Hansson, H. A. & Lindstrom, J. (1981). Osseointegrated titanium implants: requirements for ensuring a long-lasting, direct bone to implant anchorage in man. *Acta Orthopaedica Scandinavica*, *52*, pp. 155-170.

Al-Rasheed, R. A. (2005). Water treatment by heterogeneous photocatalysis an overview. *4th SWCC Acquired Experience Symposium*. Jeddah.

American Health Packaging (2015). *Calcium Acetate*. Retrieved on 15 May, 2015 from http://medlibrary.org/lib/rx/meds/calcium-acetate-8/page/2/.

Amin, M. S., Randeniya, L .K., Bendavid, A, Martin, P. J., & Preston, E. W. (2010). Apatite formation from simulated body fluid on various phases of TiO_2 thin films prepared by filtered cathodic vacuum arc deposition. *Thin Solid Films, 519(4),* pp. 1300-1306.

Anil, S., Anand, P. S., Alghamdi, H., Jansen, J. A. (2011). Turkyilmaz, I. (Ed.). Dental implant surface enhancement and osseointegration. *Implant Dentistry-A Rapidly Evolving Practice*. Crotia: Intech. pp. 83-108.

Aparicio, C., Padrós, A. & Gil, F. J. (2011). In vivo evaluation of micro-rough and bioactive titanium dental implants using histometry and pull-out tests. *Journal of the Mechanical Behavior of Biomedical Materials*, *4(8)*, pp. 1672-1682.

Augugliaro, V., Loddo, V., Pagliaro, M., Palmisano, G. & Palmisanov, L. (2010). *Clean by light irradiation: practical applications of supported TiO_2*. Cambridge: RSC Publishing.

Basu, B. & Nath, S. (2009). Fundamentals of biomaterials and biocompatibility. Basu, B., Katti, D. S. & Kumar, A. (Ed.). *Advance Biomaterials: Fundamentals, Processing and Applications*. New Jersey: John Wiley & Sons. pp. 3-18.

Bauccion, M. (1993). *ASM Metals Reference Book*. ASM International.

Bauer, S., Schmuki, P., von der Mark, K. & Park, J. (2013). Engineering biocompatible implant surfaces. *Progress in Materials Science, 58(3)*, pp. 261-326.

Bensalah, W., Feki, M., Wery, M. & Ayedi, H. F. (2011). Chemical dissolution resistance of anodic oxide layers formed on aluminum. *Transactions of Nonferrous Metals Society of China (English Edition)*, *21(7)*, pp. 1673-1679.

Bickley, R. I., Gonzalez-carreno, T., Lee, J. S., Palmisano, L. & Tilleyd, R. J. D. (1991). Investigation of titanium dioxide photocatalysts. *Journal of Solid State Chemistry*, *92*, pp. 178-190.

Bjursten, L .M. (1991). The Bone-Implant Interface in Osseointegration. *International Workshop on Osseointegration in Skeletal Reconstruction and Joint Replacement*. Sweden. pp. 25-31.

Boehm, H. P. (1971). Acidic and basic properties of hydroxylated metal oxide surfaces. *Discussion Faraday Society*, *52*, pp. 264-275.

Bohner, M., Galea, L. & Doebelin, N. (2012). Calcium phosphate bone graft substitutes: failures and hopes. *Journal of the European Ceramic Society, 32(11)*, pp. 2663-2671.

Boonchom, B. & Danvirutai, C. (2009). The morphology and thermal behavior of calcium dihydrogen phosphate monohydrate ($Ca(H_2PO_4)_2 \cdot H_2O$) obtained by a rapid precipitation route at ambient temperature in different media. *Journal of Optoelectronics and Biomedical Materials, 1(1),* pp. 115-123.

Boretos, J. W. & Eden, M. (1984). *Contemporary biomaterials, material and host response, clinical applications, new technology and legal aspects*. New Jersey: Noyes Publications.

Bornstein, M. M., Valderrama, P., Jones, A .a, Wilson, T. G., Seibl, R. & Cochran, D. L. (2008). Bone apposition around two different sandblasted and acid-etched titanium implant surfaces: a histomorphometric study in canine mandibles. *Clinical Oral Implants Research, 19(3),* pp. 233-241.

Bose, S. & Tarafder, S. (2012). Calcium phosphate ceramic systems in growth factor and drug delivery for bone tissue engineering: a review. *Acta Biomaterialia, 8(4),* pp. 140-1421.

Bouroushian, M. & Kosanovic, T. (2012). Characterization of thin films by low incidence x-ray diffraction. *Crystal Structure Theory and Applications, 1(3),* pp. 35-39.

Brånemark, R. (n.d). *Osseointegration*. Centre of Orthopaedic Osseointegration (COD), Department of Orthopaedics, Sahlgren University Hosepital, Göteborg, Sweden.

Brånemark, R., Brånemark, P., Rydevik, B. & Myers, R .R. (2001). Osseointegration in skeletal reconstruction and rehabilitation: a review. *Journal of Rehabilitation Research and Development, 38(2),* pp. 175-181.

Bumbrah, G. S. & Sharma, R. M. (2015). Raman spectroscopy-basic principle, instrumentation and selected applications for the characterization of drugs of abuse. *Egyptian Journal of Forensic Sciences*. In press.

Cai, K.Y. (2007). Surface modification of titanium films with sodium ion implantation: surface properties and protein adsorption. *Acta Metallurgica Sinica, 20(2),* pp. 148-156.

Cai, Y .L. (2013). *Titanium dioxide photocatalysis in biomaterials applications*. Uppsala University: Ph.D.'s thesis.

Cai, Y. L., Yang, X. J., Cui, Z. D., Chen, M. F., Hu, K. & Li, C. Y. (2013). Zhang, S. (Ed.). Biofuntionalization of NiTi shape memory alloy promoting osseointegration by chemical treatment. *Hydroxyapatite Coatings on Biomedical Applications*. Boca Raton: CRC Press. pp. 289-360.

Cayman Chemical (2014). β-Glycerophosphate (Sodium Salt Hydrate). Retrieved on 15 July, 2014 from https://www.caymanchem.com/app/template/ Product.vm/ catalog/14405; jsessionid=0703D30E1816E05DFFC09A1137246444.

Chai, Y. C., Carlier, A, Bolander, J., Roberts, S .J., Geris, L., Schrooten, J. & Van Oosterwyck, H. (2012). current views on calcium phosphate osteogenicity and the translation into effective bone regeneration strategies. *Acta Biomaterialia, 8(11)*, pp. 3876-3887.

Chand, P., Gaur, A. & Kumar, A. (2015). Effect of Ni doping on structural and optical properties of Cu1–*x*Ni*x*O ($0 \leq x \leq 0.20$) nanostructures. *Applied Science Letter, 1(1)*, pp. 28-32.

Chang, H. I. & Wang, Y. W. (2011). Eberli, D. (Ed.).Cell responses to surface and architecture of tissue engineering scaffolds. *Regenerative Medicine and Tissue Engineering Cells and Biomaterials.* Crotia: Intech. pp. 569-588.

Chang, Y. & Webster, T. (2006). Anodization: a promising nano-modification technique of titanium implants for orthopedic applications. *Journal of Nanoscience and Nanotechnology*, *6(9-10)*, pp. 2682-2692.

Chaudhury, M. K. (1996). Interfacial interaction between low-energy surfaces. *Material Science Engineering*. *R16*, pp. 97-159.

Chertow, G. M., Burke, S. K. & Raggi, P. (2002). Sevelamer attenuates the progression of coronary and aortic calcification in hemodialysis patients. *Kidney International*, *62*, pp. 245-252.

Chi, M. H., Tsou, H. K., Chung, C. J. & He, J. L. (2013). Biomimetic hydroxyapatite grown on biomedical polymer coated with titanium dioxide interlayer to assist osteocompatible performance. *Thin Solid Films*, *549*, pp. 98–102.

Chug, A., Shukla, S., Mahesh, L. & Jadwani S. (2013). Osseointegration-molecular events at the bone-implant interface: a review. *Journal of Oral and Maxillofacial Surgery, Medicine, and Pathology*, *25(1)*, pp. 1-4.

Chung, C. H., Golub, E. E., Forbes, E., Tokuoka, T., Shapiro, I .M. (1992). Mechanism of action of β-glycerophosphate on bone cell mineralization. *Calcified Tissue International*, *51(4)*, pp. 305-311.

Ciganovic, J., Stasic, J., Gakovic, B., Momcilovic, M., Milovanovic, D., Bokorov, M. & Trtica, M. (2012). Surface modification of the titanium implant using TEA CO_2 laser pulses in controllable gas atmospheres-Comparative study. *Applied Surface Science*, *258(7)*, pp. 2741-2748.

Cihlar, K. & Castkova, K. (1998). Synthesis of calcium phosphates from alkyl phosphates by the sol-gel method. *Ceramic-Silikaty*, *42(4)*, pp. 164-170.

Cimdina, L. B. & Borodajenko, N. (2012). Theophanides, T. (Ed.). Research of Calcium Phosphates Using Fourier Transform Infrared Spectroscopy. *Infrared Spectroscopy - Materials Science, Engineering and Technology*. Crotia: Intech. pp. 123-148.

Cui, X., Kim, H. M., Kawashita, M., Wang, L., Xiong, T., Kokubo, T. & Nakamura, T. (2009). Preparation of bioactive titania films on titanium metal via anodic oxidation. *Dental Materials : Official Publication of the Academy of Dental Materials*, *25*(1), pp. 80-86.

Dang, Q. F., Yan, J. Q., Li, J. J., Cheng, X. J., Liu, C. S. & Chen, X. G. (2011). Controlled gelation temperature, pore diameter and degradation of a highly porous chitosan-based hydrogel. *Carbohydrate Polymers*, *83(1)*, pp. 171-178.

Das, K., Bose, S. & Bandyopadhyay, A. (2007). Surface modifications and cell-materials interactions with anodized Ti. *Acta Biomaterialia*, *3(4)*, pp. 573-585.

De Souza, G. B., de Lima, G. G., Kuromoto, N. K., Soares, P., Lepienski, C. M., Foerster, C. E. & Mikowski, A. (2011). Tribo-mechanical characterization of rough, porous and bioactive Ti anodic layers. *Journal of the Mechanical Behavior of Biomedical Materials, 4(5)*, pp. 796-806.

Deligianni, D. D., Katsala, N., Ladas, S., Sotiropoulou, D., Amedee, J. & Missirlis, Y. F. (2001). Effect of surface roughness of the titanium alloy Ti-6Al-4V on human bone marrow cell response and on protein adsorption. *Biomaterials, 22(11)*, pp. 1241-1251.

Delplancke, J. L. Degrez, M., Fontana, A. & Winand, R. (1982). Self-colour anodizing of titanium. *Surface Technology, 16(2)*, 153-162.

Diamanti, M. V. & Pedeferri, M. P. (2007). Effect of anodic oxidation parameters on the titanium oxides formation. *Corrosion Science, 49(2)*, pp. 939-948. Diebold, U. (2003). The surface science of titanium dioxide. *Surface Science Report, 48 (5-8)*, pp. 53-229.

Divya, S., Nampoori, V. P. N., Radhakrishnan, P. & Mujeeb, a. (2014). Electronic and optical properties of TiO_2 and its polymorphs by Z-scan method. *Chinese Physics B*, *23*(*8*), pp. 1-5.

Durdu, S., Deniz, Ö. F., Kutbay, I. & Usta, M. (2013). Characterization and formation of hydroxyapatite on Ti6Al4V coated by plasma electrolytic oxidation. *Journal of Alloys and Compounds*, *551*, pp. 422-429.

Ehrenfest, D. M. D., Coelho, P. G., Kang, B. S., Sul, Y. T. & Albrektsson, T. (2010). Classification of osseointegrated implant surfaces: materials, chemistry and topography. *Trends in Biotechnology, 28(4)*, pp. 198-206.

Elias, C. N. (2010). Titanium dental implant surfaces. *Matéria*, *15*, pp. 138-142.

Elias, C. N., Lima, J. H. C., Valiev, R.. & Meyers, M .A. (2008a). Biomedical applications of titanium and its alloys. *Journal of Materials*, *60(3)*, pp. 46-49.

Elias, C. N., Oshida, Y., Lima, J. H. C., & Muller, C. A. (2008b). Relationship between surface properties (roughness, wettability and morphology) of titanium and

dental implant removal torque. *Journal of the Mechanical Behavior of Biomedical Materials, 1(3),* pp. 234-242.

Emmett, M. (2006), A comparison of calcium-based phosphorus binders for patients with chronic kidney disease. *Dialysis Transplantation*, *35*, pp. 284-293.

Faghihi-Sani, M. A., Arbabi, A. & Mehdinezhad-Roshan, A. (2013). Crystallization of hydroxyapatite during hydrothermal treatment on amorphous calcium phosphate layer coated by PEO technique. *Ceramics International*, *39(2),* pp. 1793-1798.

Fairley,M. (2006). Osseointegration: in the wave of the future. *The Orthotics & Prosthetics Edge*, pp. 43-46.

Farr, J. N. & Khosla, S. (2016). Determinants of bone strength and quality in diabetes mellitus in humans. *Bone*, *82*, pp. 28-34.

Gao, Y., Liu, Y., Zhou, L., Guo, Z. H., Rong, M. D. Liu, X. N., Lai, C. H. & Ding, X. L. (2012). The effects of different wavelength UV photofunctionalization on micro-arc oxidized titanium. *Chinese Journal of Stomatology*, *8*, pp. 359-363.

Geesink, R. G. T., de Groot, K. & Klein, C. P. A. T. (1987). Chemical implant fixation using hydroxyl-apatite coatings. *Clinical Orfkop*. *225*, pp. 147-170.

Geetha, M., Singh, A. K., Asokamani, R. & Gogia, A. K. (2009). Ti based biomaterials, the ultimate choice for orthopaedic implants-a review. *Progress in Materials Science, 54(3),* pp. 397-425.

Goenka, S., Balu, R. & Sampath Kumar, T. S. (2012). Effects of nanocrystalline calcium deficient hydroxyapatite incorporation in glass ionomer cements. *Journal of the Mechanical Behavior of Biomedical Materials, 7*, pp. 69-76.

Han, Y., Chen, D., Sun, J., Zhang, Y., & Xu, K. (2008). UV-enhanced bioactivity and cell response of micro-arc oxidized titania coatings. *Acta Biomaterialia, 4(5),* pp. 1518-1529.

Han, Y., Hong, S. H. & Xu, K. (2003). Structure and in vitro bioactivity of titania-based films by micro-arc oxidation. *Surface & Coatings Technology, 168*, pp. 249-258.

Hanaor, D. a. H. & Sorrell, C. C. (2011). Review of the anatase to rutile phase transformation. *Journal of Materials Science, 46*, pp. 855-874.

Hanawa, T. (2008). *Chapter 7: Implants and Biomaterials (Titanium Metal)*. Tokyo Dental and Medical Univeristy.

Harcuba, P., Bacáková, L. Stráský, J., Bacáková, M., Novotná, K. & Janecek, M. (2012). Surface treatment by electric discharge machining of Ti-6Al-4V alloy for potential application in orthopaedics. *Journal of Mechanical Behavior of Biomedical Materials, 7*, pp. 96-105.

He, W. Z., Park, S. J., Shin, D. H. Yoon, S. J., Wu, Y. Q., Qiu, J., Hwang, Y. H., Kim, H. K. & Kim, B. (2011). Effect of annealing Ti foil on the structural properties of anodic TiO_2 nanotube. *Journal of the Korean Physical Society*, *58*(*31*), pp. 575-579.

Hermawan, H. & Mantovani, D. (2009). Degradable metallic biomaterials: the concept, current developments and future directions. *Minerva Biotec*, *21*, pp. 207-216.

Hermawan, H., Ramdan, D. & Djuansjah, J. R. P. (2011). Rezai, R. F. (Ed.). Metals for biomedical application. *Biomedical Engineering-From Theory to Applications*. Croatia: Intech. pp. 411-424.

Hiromoto, S., Shishido, T., Yamamoto, A. & Maruyama, N. (2008). Precipitation control of calcium phosphate on pure magnesium by anodization. *Corrosion Science, 50(10)*, pp. 2906–2913.

Hitchman, M. L., Spackman, R. A. & Agra, C. Photoelectrochemical study of titanium dioxide films prepared by anodisation of titanium metal in sulfuric acid. *Journal of Chemical Society: Faraday Transaction, 92*, pp. 4049-4052.

Hollander, A. P. & Hatton, P. V. (2004). *Biopolymer Methods in Tissue Engineering*. New Jersey: Hamana Press Inc.

Hsu, Y. H., Turner, I. G. & Miles, A.W. (2010). A Commentary on "evaluation of the in vitro bioactivity of bioceramics." *Bone and Tissue Regeneration Insights*, pp. 1-4.

Hu, H., Zhang, W., Qiao, Y., Jiang, X., Liu, X. & Ding, C. (2012). Antibacterial activity and increased bone marrow stem cell functions of Zn-incorporated TiO_2 coatings on titanium. *Acta Biomaterialia*, *8(2)*, pp. 904-915.

Huang, P., Xu, K. and Han, Y. (2007). Formation mechanism of biomedical apatite c coatings on porous titania layer. *Journal of Materials Science Material in Medicine*, *18 (3)*, pp. 457-463.

Huang, X. & Liu, Z. (2013). Growth of titanium oxide or titanate nanostructured thin films on Ti substrates by anodic oxidation in alkali solutions. *Surface and Coatings Technology*, *232*, pp. 224-233.

Ishizawa, H. & Ogino, M. (1995). Formation and characterization of anodic titanium oxide films containing Ca and P. *Journal of Biomedical Materials Research*, *29*, pp. 65-72.

Jalota, S (2007). *Development and in vitro examination of materials for osseointegration*. Clemson University: Ph.D.'s Thesis.

Jeevithan, E., Jeya Shakila, R., Varatharajakumar, a., Jeyasekaran, G. & Sukumar, D. (2013). Physico-functional and mechanical properties of chitosan and calcium salts incorporated fish gelatin scaffolds. *International Journal of Biological Macromolecules*, *60*, pp. 262-267.

Jeong, Y. H., Kim, E. J., Brantley, W. a. & Choe, H. C. (2014). Morphology of hydroxyapatite nanoparticles in coatings on nanotube-formed Ti–Nb–Zr alloys for dental implants. *Vacuum*, *107*, pp.297-303.

Kamboj, M. L. (2009). *Studied on the degradation of industrial waste water using heterogeneous photocatalysis*. Thapar University: Master's Thesis.

Kaneko, M., Okura, I. (2002). *Photocatalysis: science and technology*. 1st edition. New York: Springer Publishing.

Kasuga, T., Kondo, H. & Nogami, M. (2002). Apatite formation on TiO_2 in simulated body fluid. *Journal of Crystal Growth*, *235(1-4)*, pp. 235-240.

Khor, K. A., Yip, C. S. & Cheang, P. (1997). Ti-6Al-4V/hydroxyapatite Composite coating preapred by thermal spray techniques. *Journal of Thermal Spray Technology*, *6(1)*, pp. 109-115.

Kim, K. H. & Ramaswamy, N. (2009). Electrochemical surface modification of titanium in dentistry. *Dental materials journal*, *28(1)*, pp. 20-36.

Kim, M. S., & Kim, Y. J. (2012). Synthesis of calcium-deficient hydroxyapatite in the presence of amphiphilic triblock copolymer. *Materials Letters*, *66(1)*, pp. 33-35.

Kim, S. E., Lee, S. B., Kwak, S. W., Kim, C. K. & Kim, K. N. (2012), Nanoporous anodic oxidation titanium enhances cell proliferation and differentiation of immortalized mouse embryonic cells. *Surface & Coating Technology*, *228*, pp. 537-540.

Koelsch, M., Cassaignon, S., Ta, T. M., Guillemoles, J. F. & Jolivet, J. P. (2004). Electrochemical comparative study of titania (anatase, brookite and rutile) nanoparticles synthesized in aqueous medium. *Thin Solid Films*, *451-452*, pp, 86-92.

Kokubo, T. (1998). Apatite formation on surfaces of ceramics, metals and polymers in body environment. *Acta Materialia*, *46(7)*, pp. 2519-2527.

Kokubo, T., & Takadama, H. (2006). How useful is SBF in predicting in vivo bone bioactivity?. *Biomaterials*, *27(15)*, pp. 2907-2915.

Kokubo, T., Kim, H. M., Takadama, H., Uchida, M., Nishiguchi, S. & Nakamura, T. (2000). Mechanism of apatite formation on bioactive titanium metal. *Materials Research Society Symposium Proceedings*. Boston. pp. 129-134.

Kong, J., Wang, Y., Wang, Z. & Jia, H. (2016). Preparation and photocatalytic activity of carbon coating TiO_2 nanotubes. *Superlattices and Microstructures*, *89*, pp. 252-258.

Kovan, V. (2008). An assessment of impact strength of the mandible. *Journal of Biomechanics, 41(16),* pp. 3488-3491.

Krupa, D., Baszkiewicz, J., Sobczak, J. ., Biliński, A. & Barcz, A. (2003). Modifying the properties of titanium surface with the aim of improving its bioactivity and corrosion resistance. *Journal of Materials Processing Technology, 143-144,* pp. 158-163.

Kumar, C. (2013). *Surface modification of Ti-6Al-4V by electrochemical oxidation*. National Institute of Technology Rourkela: Master's Thesis.

Lan, Y. C., Lu, Y. L. & Ren, Z. F. (2013). Mini review on photocatalysis of titanium dioxide nanoparticles and their solar applications. *Nano Energy, 2,* pp. 1031-1045.

Lane, W. A. (1895). Some remarks on the treatment of fractures. *Journal of British Medical,* pp. 861-863.

Le Guehennec, L., Lopez-Heredia, M. A., Enkel, B., Weiss, P., Amouriq, Y. & Layrolle, P. (2008). Osteoblastic cell behaviour on different titanium implant surfaces. *Acta Biomaterialia, 4(3),* pp. 535-543.

Lecanda, F., Avioli, L.V. & Cheng, S. (1992). Regulation of bone matrix protein expression and induction of differentiation of human osteoblasts and human bone marrow stromal cells by bone morphogenetic protein-2. *Journal of Cell Biochemistry, 67(3),* pp. 386-396.

Lee, T. C., Abdullah, H. Z. & Idris, M. I. (2015c). Mechanism of bone-like apatite formation on anodised titanium under UV irradiation. *Proceedings of the 3rd International Conference on Advances in Civil, Structural and Mechanical Engineering (CSM 2015)*. Birmingham City University: Seek Digital Library. pp. 51-55.

Lee, T. C., Abdullah, H. Z. & Idris, M. I. (2015e). Effect of UV wavelength on apatite formation of anodised titanium. *Advanced Materials Research, 1125,* pp. 465-469.

Lee, T. C., Idris, M. I., Abdullah, H. Z. & Sorrell, C. C. (2015a). Effect of electrolyte concentration on anodised titanium in mixture of β-glycerophosphate (β-GP) and calcium acetate (CA). *Advanced Materials Research, 1087*, pp. 116-120.

Lee, T. C., Koshy, P., Abdullah, H. Z. & Idris, M. I. (2015d). Precipitation of bone-like apatite on anodised titanium in simulated body fluid under UV irradiation. *Surface & Coating Technology*, In Press.

Lee, T. C., Rathi, M. F. M., Abidin, M. Y. Z., Abdullah, H. Z. & Idris, M. I. (2015b). Effect of applied voltage on surface properties of anodised titanium in mixture of β-glycerophosphate (β-GP) and calcium acetate (CA). *Proceedings of the 23rd Scientific Conference of Microscopy Society Malaysia (SCMSM 2014)*. Universiti Teknologi Petronas: AIP Publishing.

Leeds, S. M. (1999). *Characterisation of the gas-phase environment in a microwave plasma enhanced diamond chemical vapour deposition reactor using molecular beam mass spectrometry*. University of Bristol: Ph.D.'s Thesis.

Legeros, R. Z., Ito, A., Ishikawa, K., Sakae, T. & John, P. L. (2009). Basu, B., Katti, D. S. & Kumar, A. (Ed.). Fundamental of hydroxyapatite and related calcium phosphates. *Advance Biomaterials: Fundamentals, Processing and Applications*. New Jersey: John Wiley & Sons. pp. 19-52.

LeGuéhennec, L., Soueidan, A., Layrolle, P. & Amouriq, Y. (2007). Surface treatments of titanium dental implants for rapid osseointegration. *Dental Materials, 23(7)*, pp. 844-854.

Li, J., Wang, X., Hu, R. & Kou, H. (2014). Structure, composition and morphology of bioactive titanate layer on porous titanium surfaces. *Applied Surface Science, 308*, pp. 1-9.

Li, L. H., Kong, Y. M., Kim, H. W., Kim, Y. W., Kim, H. E., Heo, S. J. & Koak, J. Y. (2004). Improved biological performance of Ti implants due to surface modification by micro-arc oxidation. *Biomaterials, 25(14)*, pp. 2867-2875.

Liang, F., Zhou, L. & Wang, K. (2003). Apatite formation on porous titanium by alkali and heat-treatment. *Surface and Coatings Technology*, *165(2)*, pp. 133-139.

Lilley, P.A., Walker, P.S. & Blunn, G.W. (1992). Wear of titanium by soft tissue. *Transactions of the 4th Word Biomaterials Congress*. Berlin, pp. 227-230.

Liu, F., Wang, F., Shimizu, T., Igarashi, K. & Zhao, L. (2006). Hydroxyapatite formation on oxide films containing Ca and P by hydrothermal treatment. *Ceramics International*, *32*(5), pp. 527-531.

Liu, F., Xu, J., Wang, F., Zhao, L. & Shimizu, T. (2010). Biomimetic deposition of apatite coatings on micro-arc oxidation treated biomedical NiTi alloy. *Surface & Coatings Technology, 204(20)*, pp. 3294-3299.

Liu, R. S. (2012). *Controlled nanofabrication: advances and applications*. Singapore: Pan Stanfold Publishing Pte. Ltd.

Liu, X., Chu, P., & Ding, C. (2004). Surface modification of titanium, titanium alloys, and related materials for biomedical applications. *Materials Science and Engineering*, *47*, pp. 49-121.

Long, M. J. & Rack, H. J. (1998). Titanium alloys in total joint replacement-a materials science perspective. *Biomaterials, 19(18)*, pp. 1621-1639.

Maecker, H. (2009). *The Electric Arc*. H Popp Matlab GmbH.

Manivasagam, G., Dhinasekaran, D. & Rajamanickam, A. (2010). Biomedical implants: corrosion and its prevention-a review. *Recent Patents on Corrosion Science*, *2*, pp. 40-54.

Mantz, R. (2010). *Semiconductor electrolyte interface and photoelectrochemistry*. New Jersey: ECS Transaction.

Marques, M. R C., Loebenberg, R., & Almukainzi, M. (2011). Simulated biological fluids with possible application in dissolution testing. *Dissolution Technologies*, 18, pp. 15-28.

Martini, C., & Ceschini, L. (2011). A comparative study of the tribological behaviour of PVD coatings on the Ti-6Al-4V alloy. *Tribology International, 44(3),* pp. 297-308.

Mavrogenis, A. F., Dimitriou, R., Parvizi, J. & Babis, G. C. (2009). Biology of implant osseointegration. *Journal of Musculoskelet Neuronal Interact, 9(2),* pp. 61-71.

Milne, G.W.A. (2005). *Gardner's Commercially Important Chemicals: Synonyms, Trade Names, and Properties*. New Jersey: John Wiley & Sons.

Mizukoshi, Y. & Masahashi, N. (2014). Fabrication of a TiO_2 photocatalyst by anodic oxidation of Ti in an acetic acid electrolyte. *Surface and Coatings Technology, 240,* pp. 226-232.

Mohammad, M. T., Khan, Z. A. & Siddiquee, A. N. (2012). Titanium and its alloys, the imperative materials for biomedical applications. *Proceedings International. Conference on Recent Trends in Engineering & Technology.* Meerut, India. pp. 91-95.

Montazeri, M., Dehghanian, C., Shokouhfar, M. & Baradaran, A. (2011). Investigation of the voltage and time effects on the formation of hydroxyapatite-containing titania prepared by plasma electrolytic oxidation on Ti-6Al-4V alloy and its corrosion behavior. *Applied Surface Science, 257(16),* pp. 7268-7275

Morris, C. G. (1992). *Academic Press Dictionary of Science and Technology*. California: Academic Press, Inc

Nag, S. & Banerjee, R. (2012). Fundamental of medical implant materials. *ASM Handbook: Materials for Medical Devices, 23*, pp. 6-17.

Nallaswamy, D. (2008). *Textbook of Prosthodontics.* New Delhi: Jaypee Brothers Publishers.

Nan, Y. (2007). *Focused Ion Beam Systems: Basics and Applications 2011*. Cambridge University Press.

Nascimento, C. D., Issa, J. P. M., Oliveira, R. R. D., Iyomasa, M. M., Siéssere, S. & Regalo, S. C. H. (2007). Biomaterials applied to the bone healing process. *International Journal of Morphology, 58(3),* pp. 839-846.

Nath, S. & Basu, B. (2009). Materials for orthopedic application. Basu, B., Katti, D. S. & Kumar, A. (Ed.). *Advance Biomaterials: Fundamentals, Processing and Applications*. New Jersey: John Wiley & Sons. pp. 53-100.

Necula, B. S., Apachitei, I., Fratila-Apachitei, L. E., van Langelaan, E. J. & Duszczyk, J. (2013). Titanium bone implants with superimposed micro/nano-scale porosity and antibacterial capability. *Applied Surface Science, 273*, pp. 310-314.

Neupane, M. P., Park, I.S ., Bae, T. S. & Lee, M. H. (2013). Sonochemical assisted synthesis of nano-structured titanium oxide by anodic oxidation. *Journal of Alloys and Compounds, 581*, pp. 418-422.

Nishiguchi, S., Kato, H., Fujita, H., Oka, M., Kim, H. M., Kokubo, T., & Nakamura, T. (2001). Titanium metals form direct bonding to bone after alkali and heat treatments. *Biomaterials, 22(18),* pp. 2525-2533.

Ogawa, T. & Nishimura, I. (2003). Different bone integration profiles of turned and acid etched implants associated with Modulated expression of extracellular matrix genes. *International Journal of Oral Maxillofacial Implants, 18(2),* pp. 200 -210.

Oh, H. J., Lee, J. H., Jeong, Y., Kim, Y. J. & Chi, C. S. (2005). Microstructural characterization of biomedical titanium oxide film fabricated by electrochemical method. *Surface and Coatings Technology, 198(1-3),* pp. 247-252.

Ohtsu, N., Kozuka, T., Hirano, M. & Arai, H. (2015). Electrolyte effects on the surface chemistry and cellular response of anodized titanium. *Applied Surface Science, 349*, pp. 911-915.

Oldani, C. & Dominguez, A. (2012). Fokter, S. K. (Ed.). Titanium as a biomaterial for implants. *Recent Advances in Arthroplasty*. Croatia: Intech. pp. 149-162.

Ono, S., Kiyotake, A. & Asoh, H. (2008). Effect of nanostructured surfaces of light metals on hydroxyapatite coating. *ESC Transactions, 11(15)*, pp. 1-8.

Oshida, Y., Tuna, E. B., Aktoren, O. & Gencay, K. (2010). Dental implant systems. *International Journal of Molecular Sciences, 11(4)*, pp. 1580-1678.

Ou, S. F., Chou, H. H., Lin, C. S., Shih, C. J., Wang, K. K. & Pan, Y. N. (2012). Effects of anodic oxidation and hydrothermal treatment on surface characteristics and biocompatibility of Ti-30Nb-1Fe-1Hf alloy. *Applied Surface Science*, *258(17)*, pp. 6190-6198.

Ou, S. F., Lin, C. S. & Pan, Y. N. (2011). Microstructure and surface characteristics of hydroxyapatite coating on titanium and Ti-30Nb-1Fe-1Hf alloy by anodic oxidation and hydrothermal treatment. *Surface and Coatings Technology*, *205(8-9)*, pp. 2899-2906.

Özcan, M., & Hämmerle, C. (2012). Titanium as a reconstruction and implant material in dentistry: advantages and pitfalls. *Journal of Materials, 5(12)*, pp. 1528-1545.

Paital, S. R. & Dahotre, N. B. (2009). Wettability and kinetics of hydroxyapatite precipitation on a laser-textured Ca-P bioceramic coating. *Acta Biomaterialia*, *5(7)*, pp. 2763–2772.

Pan, Y. K., Chen, C. Z., Wang, D. G. & Lin, Z. Q. (2013). Preparation and bioactivity of micro-arc oxidized calcium phosphate coatings. *Materials Chemistry and Physics, 141(2-3)*, pp. 842-849.

Park, J. B. (1984). *Biomaterials sciences and enginnering*. New York: Plenum Press.

Park, K. H., Koak, J. Y., Kim, S. K. & Heo, S. J. (2011). Wettability and cellular response of UV light irradiated anodized titanium surface. *The Journal of Advanced Prosthodontics*, *3(2)*, pp. 63-68.

Park, T. E., Choe, H. C. & Brantley, W. A. (2013). Bioactivity evaluation of porous TiO_2 surface formed on titanium in mixed electrolyte by spark anodisation. *Surface & Coating Technology*, *235*, pp. 706-713

Patel, N. R. & Gohil, P. P. (2012). A review on biomaterials: scope, applications & anatomy significance. *International Journal of Emerging Technology and Advanced Engineering, 2(4)*, pp. 91-101.

Perry, D. L. (2011). *Handbook of Inorganic Compounds*. 2nd Edition. Florida: CRC Press.

Popa, M., Vasilescu, C., Drob, S. I., Osiceanu, P., Anastasescu, M. & Calderon-Moreno, J. M. (2013). Characterization and corrosion resistance of anodic electrodeposited titanium oxide/phosphate films on Ti-20Nb-10Zr-5Ta bioalloy. *Journal of the Brazilian Chemical Society, 24(7)*, pp. 1123-1134.

Ramazanoglu, M. & Oshida, Y. (2011). Turkuilmaz, I.(Ed.). Osseointegration and bioscience of implant surfaces-current concepts at bone-implant interface *Implant Dentistry-A Rapidly Evolving Practice*. Crotia: Intech. pp. 57-82.

Ratnawati, Gunlazuardi, J., & Slamet. (2015). Development of titania nanotube arrays: The roles of water content and annealing atmosphere. *Materials Chemistry and Physics, 160*, pp. 111-118.

Ratner, B. D. & Bryant, S. J. (2004). Biomaterials: where we have been and where we are going. *Annual Review of Biomedical Engineering, 6*, pp. 41-75.

Ravelingien, M., Mullens, S., Luyten, J., Meynen, V., Vinck, E., Vervaet, C. & Remon, J. P. (2009). Thermal decomposition of bioactive sodium titanate surfaces. *Applied Surface Science, 255(23)*, pp. 9539-9542.

Rouquerol, J., Rouquerol, F., Llewellyn, P., Maurin, G. & Sing, K. S. W. (2013). *Adsorption by powders and porous solids: principles, methodology and applications*. 2nd Edition. United State: Academic Press.

Saha, N. (2012). *Investigation on the synthesis and optical properties of nanostructured $ZnWO_4$*. Jadavpur University: Master's Thesis.

Samavedi, S., Whittington, A. R. & Goldstein, A. S. (2013). Calcium phosphate ceramics in bone tissue engineering: a review of properties and their influence on cell behavior. *Acta Biomaterialia, 9(9)*, pp. 8037-8045.

Schuler, M., Owen, G. R., Hamilton, D. W., de Wild, M., Textor, M., Brunette, D. M. & Tosatti, S. G. P. (2006). Biomimetic modification of titanium dental implant model surfaces using the RGDSP-peptide sequence: a cell morphology study. *Biomaterials, 27(21),* pp. 4003-4015.

Shabani, M. & Zamiri, R. (2014). Effect of applied voltage and substrate preparation on surface modification of anodically oxidized titanium. *Journal of Ovanic Research, 10,* pp. 43-53.

Shadanbaz, S., & Dias, G. J. (2012). Calcium phosphate coatings on magnesium alloys for biomedical applications : a review. *Acta Biomaterialia, 8(1),* pp. 20-30.

Shimohigoshi, M. & Saeki, Y. (2007). Research and applications of photocatalyst tiles. *Photocatalysis, Environment and Construction Materials, 55,* pp. 291-298.

Shioi, A., Nishizawa, Y., Jono, S., Koyama, H., Hosoi, M. & Morii, H. (1995). β-Glycerophosphate accelerates calcification in cultured bovine vascular smooth muscle cells. *Arteriosclerosis, Thrombosis, and Vascular Biology, 15(11),* pp. 2003-2009.

Si, H. Y., Sun, Z.H., Kang, X., Zi, W. W. & Zhang, H. L. (2009). Voltage-dependent morphology, wettability and photocurrent response of anodic porous titanium dioxide films. *Microporous and Mesoporous Materials, 119(1-3),* pp. 75-81.

Sigma Aldrich (2013). β-Glycerophosphate Disodium Salt Hydrate. Retrieved on 18 September, 2013 from http://www.sigmaaldrich.com/catalog/product/sigma/g9891? lang=en&region=MY.

Simka, W., Socha, R. P., Dercz, G., Michalska, J., Maciej, A. & Krząkała, A. (2013). Anodic oxidation of Ti-13Nb-13Zr alloy in silicate solutions. *Applied Surface Science, 279,* pp. 317-323.

Singh, A. R. (2008). *Study of photocatalytic behaviour of TiO_2 nanopowder*. Thapar University: Master's thesis.

Song, W., Jun, Y., Han, Y. & Hong, S. (2004). Biomimetic apatite coatings on micro-arc oxidized titania. *Biomaterials, 25(17),* pp. 3341-3349.

Sul, Y. T., Johansson, C. B., Jeong, Y. S. & Albrektsson, T. (2001). The electrochemical oxide growth behaviour on titanium in acid and alkaline electrolytes. *Medical Engineering & Physics, 23(5),* pp. 329-326.

Sumner, D. & Galante, J. (1992). Determinants of stress shielding: design versus materials versus interface. *Clinical Orthopaedics and Related Research*, *247*, pp. 202-212.

Sun, J., Han, Y. & Huang, X. (2007). Hydroxyapatite coatings prepared by micro-arc oxidation in Ca- and P-containing electrolyte. *Surface and Coatings Technology*, *201*(*9-11 SPEC. ISS.),* pp. 5655-5658.

Sun, X., Jiang, Z., Yao, Z. & Zhang, X. (2005). The effects of anodic and cathodic processes on the characteristics of ceramic coatings formed on titanium alloy through the MAO coating technology. *Applied Surface Science, 252(2),* pp. 441-447.

Sundgren, J. E., Bodö, P. & Lundström, I. (1986). Auger electronspectroscopic studies of the interface between human tissue and implants of titanium and stainless steel. J*ournal of Colloid and Interface Science*, *110*, pp. 9-20.

Szesz, E. M., Pereira, B. L., Kuromoto, N. K., Marino, C. E. B., de Souza, G. B. & Soares, P. (2013). Electrochemical and morphological analyses on the titanium surface modified by shot blasting and anodic oxidation processes. *Thin Solid Films*, *528*, pp. 163-166.

Takadama, H., Kim H. M., Kokubo, T. & Nakamura, T. (2001). TEM-EDX study of mechanism of bonelike apatite formation on bioactive titanium metal in simulated body fluid. *Journal of Biomedical Material, 57(3),* pp. 441-448.

Tang, G., Zhang, R., Yan, Y. & Zhu, Z. (2004). Preparation of porous anatase titania film. *Materials Letters, 58(12-13),* pp. 1857-1860.

Vasantkumar, C. V. R. & Mansingh, A. (1990). Properties of RF sputtered tetragonal and hexagonal barium titanate films. *7th International Symposium on Applications of Ferroelectric*. Urbana-Champaign: IEEE.

Vázquez, U. O. M., Shinoda, W., Moore, P. B., Chiu, C., & Nielsen, S. O. (2009). Calculating the surface tension between a flat solid and a liquid: a theoretical and computer simulation study of three topologically different methods. *Journal of Mathematical Chemistry, 45(1),* pp. 161-174.

Wang, C. X. & Wang, M. (2002). Electrochemical impedance spectroscopy study of the nucleation and growth of apatite on chemically treated pure titanium. *Materials Letters, 54(1),* pp. 30-36.

Wang, X. J., Li, Y .C., Lin, J. G., Yamada, Y., Hodgson, P .D. & Wen, C. E. (2008). In vitro bioactivity evaluation of titanium and niobium metals with different surface morphologies. *Acta biomaterialia, 4(5),* pp. 1530-1535.

Wei, D., Zhou, Y., Jia, D. & Wang, Y. (2007a). Characteristic and in vitro bioactivity of a microarc-oxidized TiO_2-based coating after chemical treatment. *Acta Biomaterialia, 3(5),* pp. 817-827.

Wei, D., Zhou, Y., Jia, D. & Wang, Y. (2008). Biomimetic apatite deposited on microarc oxidized anatase-based ceramic coating. *Ceramics International, 34(5),* pp. 1139-1144.

Wei, D., Zhou, Y., Wang, Y. & Jia, D. (2007b). Characteristic of microarc oxidized coatings on titanium alloy formed in electrolytes containing chelate complex and nano-HA. *Applied Surface Science, 253(11),* pp. 5045-5050.

Wennerberg, A. & Alberktsson, T. (2009). Effects of titanium surface topography on bone integration: a systematic review. *Clinical Oral Implants Research. 20,* pp. 172-184.

Wiberg, E. & Wiberg, N. (2001). *Inorganic Chemistry*. Florida: Academic Press.

Williams, D. F. & Cunningham, J. (1979). *Materials in clinical dentistry*. Oxford: Oxford University Press.

Wilson, R. A. & Bullen, H. A. (2006). *Introduction to scanning probe microscopy (SPM) basic theory atomic force microscopy (AFM)*. Northern Kentucky University

Winkler, J. (2003). *Titanium dioxide*. Germany: Vincentz.

Wu, C., Ramaswamy, Y., Gale, D., Yang, W., Xiao, K., Zhang, L., Yin, Y. (2008). Novel sphene coatings on Ti-6Al-4V for orthopedic implants using sol-gel method. *Acta Biomaterialia*, *4(3)*, pp. 569-576.

Xiong, T., Cui, X., Kim, H., Kawashita, M., Kokubo, T., Wu, J. & Nakamura, T. (2004). Effect of surface morphology and crystal structure on bioactivity of titania films formed on titanium metal via anodic oxidation in sulfuric acid solution. *Key Engineering Materials*, *256*, pp. 375-378.

Yerokhin, A. L., Nie, X., Leyland, A., Matthews, A. & Dowey, S. J. (1999). Plasma electrolysis for surface engineering. *Surface & Coatings Technology*, *122(2)*, pp. 73-93.

Yu, Y., Xie, L., Chen, M., Wang, N. & Wang, H. (2015). Surface & Coatings Technology Surface characteristics and adhesive strength to epoxy of three different types of titanium alloys anodized in NaTESi electrolyte. *Surface & Coatings Technology*, *280*, pp. 122-128.

ZAPP Materials Engineering (2012). *Specialty materials titanium grade 1-4*. Germany: ZAPP.

Zhang, P., Zhang, Z., Li, W. & Zhu, M. (2013). Effect of Ti-OH groups on microstructure and bioactivity of TiO_2 coating prepared by micro-arc oxidation. *Applied Surface Science*, *268*, pp. 381-386.

Zhang, X. D. (2007). Osteoinduction and ostogenic genes expression regulated by Ca-P bioceramics. Tateishi, T. (Ed.). *Biomaterials in Asia.* Singapore: World Scientific Publishing Company. pp. 24-34.

Zhang, Y (2010). *Laser Induced Selective Activation For Subsequent Autocatalytic Electroless Plating*. Technical University of Denmark: Ph.D.'s Thesis.

Zhao, G. L., Li, X., Xia, L., Wen, G., Song, L., Wang, X. Y. & Wu, K. (2010). Structure and apatite induction of a microarc-oxidized coating on a biomedical titanium alloy. *Applied Surface Science*, *257(5)*, pp. 1762-1768.

Zhao, X., Liu, X., You, J., Chen, Z. & Ding, C. (2008). Bioactivity and cytocompatibility of plasma-sprayed titania coating treated by sulfuric acid treatment. *Surface and Coatings Technology*, *202*(14), pp. 3221-3226.

Zhao, Y. L. (2013). *The bandgap, fermi level, electronic and magnetic properties of transparent conducting oxides*. National University of Singapore: Ph.D.'s Thesis.

Zheng, M., F., D., Li, X. K., Zhang, J. B. & Liu, Q. B. (2010). Microstructure and in vitro bioactivity of laser-cladded bioceramic coating on titanium alloy in a simulated body fluid. *Journal of Alloys and Compounds*, *489(1)*, pp. 211-214.

Zheng, X., Huang, M. & Ding, C. (2000). Bond strength of plasma-sprayed hydroxyapatite/Ti composite coatings, *Biomaterials*, *21(8)*, pp. 841-849.

Zheng, Y., Xiong, C. & Zhang, L. (2014). Formation of bone-like apatite on plasma-carboxylated poly(etheretherketone) surface. *Materials Letters*, *126*, pp. 147-150.

Zhou, H. Y., Jiang, L. J., Cao, P. P., Li, J. B. & Chen, X. G. (2015). Glycerophosphate-based chitosan thermosensitive hydrogels and their biomedical applications. *Carbohydrate Polymers*, *117*, pp. 524-536.

Zhu, X., Kim, K. H. & Jeong, Y. (2001). Anodic oxide films containing Ca and P of titanium biomaterial. *Biomaterials*, *22(16)*, pp. 2199-2206.